Optical Characterization of ZnSe by Photoluminescence

by

Jody L. House

Submitted to the Department of Electrical Engineering and Computer Science
in partial fulfillment of the requirements for the degree of

Master of Science

at the

MASSACHUSETTS INSTITUTE OF TECHNOLOGY

February 1994

© Massachusetts Institute of Technology 1994. All rights reserved.

Author ....
Department of Electrical Engineering and Computer Science
January 15, 1994

Certified by ....
Leslie A. Kolodziejski
Associate Professor of Electrical Engineering
Thesis Supervisor

Accepted by ....
F. R. Morganthaler
Chairman, Departmental Committee on Graduate Students

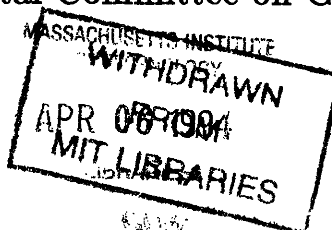
MASSACHUSETTS INSTITUTE
WITHDRAWN
APR 06 1994
MIT LIBRARIES

Optical Characterization of ZnSe by Photoluminescence

by

Jody L. House

Submitted to the Department of Electrical Engineering and Computer Science
on January 15, 1994, in partial fulfillment of the
requirements for the degree of
Master of Science

Abstract

Photoluminescence is used to optically characterize epitaxially-grown ZnSe. The ZnSe has been grown by three different growth techniques; molecular beam epitaxy, metalorganic molecular beam epitaxy and gas source molecular beam epitaxy. Photoluminescence measurements have been made for each growth method for a wide range of growth parameters. The effects of the growth parameters, as well as the constitutive sources, on the optical properties of ZnSe are compared. The resulting trends indicate that growth parameters such as the substrate temperature and the source fluxes affect both the energies and the relative intensities of the PL features, independent of the sources. However, due to the native impurities in the sources used in the epitaxial growth of ZnSe, the sources dictate the properties of the corresponding photoluminescence.

Thesis Supervisor: Leslie A. Kolodziejski
Title: Associate Professor of Electrical Engineering

Acknowledgments

I would like to thank Professor Leslie Kolodziejski for her patience and advice throughout this endeavor. As well, I would like to thank Dr. Gale Petrich for his guidance and all around help.

My mother, father, sister and brother have been with me through it all. Thanks to each one of you for your support, faith, and humor. Of course, my friends and my cats have added to the success of this project as well. I would like to thank Steve and Cabot for helping me to stay grounded in reality.

Finally, I would like to acknowledge the other members of my research group; Chris Coronado, Easen Ho, Phil Fisher, Kan Lu, Jay Damask, Kuo-Yi Lim, Joe Ahadian, and James Geraci.

The joy in the completion of my thesis is overshadowed by a great loss. I dedicate this thesis to the person I had wanted more than anyone else in the world to have seen me earn a degree from MIT, James House. I hope you are having an unusual day.

Contents

1 Introduction 1

2 Background 3

2.1 **Molecular beam epitaxy** 3

2.1.1 Variations on MBE 4

2.2 **The Physical System** 5

2.2.1 The Chambers 7

2.2.2 The Reactors 7

2.2.3 Reflection High Energy Electron Diffraction 8

2.2.4 Laser-Assisted Growth 9

2.3 **Theory of Photoluminescence** 9

2.3.1 Absorption Coefficient in a Semiconductor 10

2.3.2 Energy Bands in Semiconductors 12

2.3.3 Strain in Heterostructures 14

2.4 **Impurities, Excitons, Phonons** 16

3 Experimental 19

3.1 **Photoluminescence Set-Up** 19

3.1.1 Optical Pumping 20

3.1.2 Optical Detection 21

3.1.3 Data Acquisition 21

3.2 **System Calibration** 22

3.3 **System Limitations** 23

4 Results and Discussion **25**

4.1 **MOMBE Growth** 27

4.1.1 ZnSe Growth with DEZn and DESe Sources 30

4.1.2 ZnSe Grown with One Diethyl-Based Source and One Elemental Source 38

4.1.3 ZnSe Grown with One Dimethyl-based Source 42

4.2 **ZnSe Grown by MBE** 49

4.3 **ZnSe Grown by GSMBE** 49

4.4 **Doping of ZnSe** 58

4.4.1 ZnSe:N 60

4.4.2 ZnSe:Cl 65

5 Summary **68**

List of Figures

2-1 An overhead view of the Chemical Beam Epitaxy system. 6
2-2 The absorption of photons corresponding to the wavelength of the laser used in the PL experiment (3250 Å) as a function of depth into the ZnSe. 12
2-3 The energy band structure for a direct gap semiconductor such as ZnSe. 13
2-4 The manifestation of strain in a direct gap semiconductor such as ZnSe; (a) unstrained, (b) biaxial tension, (c) biaxial compression. 16
2-5 The energy band structure at k=0 for (a) impurities and (b) free excitons. 17

3-1 The photoluminescence set-up. 20
3-2 The PL of a ZnSe film at several different laser excitation power densities. 23
3-3 The PL of a bulk-grown ZnSe sample showing feature energies and the FWHM realizable for the experimental apparatus. 24

4-1 Photoreflection of ZnSe epilayers at T=10 K. Thickness dependence of the resonance energy and the half-width of the heavy hole exciton [27]. 26
4-2 The peak position of bound exciton emission lines and free exciton as a function of the substrate temperature [14]. 27
4-3 PL of ZnSe grown by MOMBE at several points on the sample surface. 29
4-4 Enhancement ratio for ZnSe grown using DEZn and DESe with different laser illumination energies. The line is drawn to aid the eye. The arrow denotes the bandgap energy at growth temperatures [7]. 31

4-5 PL of ZnSe grown using DEZn and DESe with different laser illumination energies. (a) 7800 Å, (b) and (c) 5145 Å, (d) and (e) 4880 Å, (f) and (g) 4579 Å, (h) and (i) 3511-3638 Å. The intensities were not normalized. 32
4-6 PL of ZnSe grown using DEZn and DESe with different substrate temperatures (T_{sub}). (a) 250°C, (b) and (c) 355°C, (d) and (e) 460°C. All of the nl samples are pseudomorphic. 34
4-7 PL of ZnSe grown using DEZn and DESe with different Zn fluxes. (a) and (b) 2 sccm, (c) and (d) 1 sccm, (e) and (f) 0.5 sccm. The nl samples are pseudomorphic to the GaAs. 37
4-8 PL of ZnSe grown using DEZn and elemental Se. 39
4-9 PL of ZnSe grown using Zn and DESe with different substrate temperatures and Zn fluxes. (a) T_{sub} = 235°C, T_{Zn}=360°C, (b) T_{sub} = 280°C, T_{Zn} = 335°C, (c) T_{sub} = 300° C, T_{Zn} = 440° C. 41
4-10 PL of ZnSe grown using DMZn and elemental Se with different substrate temperatures, (T_{sub}). (a) and (b) 330°C, (c) and (d) 310°C, (e) and (f) 280°C. 43
4-11 PL of ZnSe grown using DMZn and elemental Se with different Zn fluxes (a) and (b) 1 sccm, (c) and (d) 1.5 sccm, (e) and (f) 2 sccm. . 45
4-12 PL of ZnSe grown using DMZn and DESe. 47
4-13 PL of ZnSe grown using DMZn and H_2Se for different growth temperatures, (T_{sub}). (a) 200°C, (b) 220°C, (c) 250°C, (d) 310°C. 48
4-14 PL of ZnSe grown using elemental Zn and elemental Se. 50
4-15 (a) PL of a GSMBE sample. (b) The peak energies and FWHM's of the PL at the respective locations on the sample. 51
4-16 (a) Integrated intensity of a GSMBE-grown ZnSe film as a function of PL measurement temperature. (b) PL of GSMBE-grown ZnSe film used for the integrated intensity measurement. 53
4-17 PL of ZnSe grown using solid Zn and and H_2Se with different substrate temperatures. PL measurements made (a) at 10 K, (b) at 77 K. . . . 55

4-18 PL of ZnSe grown using solid Zn and and H_2Se with different cracking cell temperatures.(a) 600°C (b) 700°C, (c) 800°C. 57
4-19 PL of ZnSe grown using solid Zn and and H_2Se with different Zn fluxes. (a) 0.73 Å/sec (b) 0.68 Å/sec (a) 0.55 Å/sec. 59
4-20 PL of ZnSe:N grown by GSMBE with different RF powers. (a) 300 W, (b) 200 W, (c) 100 W. 61
4-21 PL of ZnSe:N grown by GSMBE with different N_2 background pressures. (a)$2.1x10^{-5}$ Torr, (b) $9.7x10^{-6}$ Torr (c)$4.5x10^{-6}$ Torr. 63
4-22 (a) Plot of the energy of the donor-acceptor-pair transition in the PL of nitrogen doped ZnSe. (b) Flat band depiction of deep and shallow nitrogen donor levels in ZnSe [30]. 64
4-23 PL of ZnSe:Cl grown by GSMBE with different $ZnCl_2$ cell temperatures (a) 150°C, (b) 170°C, (c) 190°C. 66
4-24 Plot of the intensity of the donor-bound exciton feature in the PL of chlorine-doped ZnSe. 67

List of Tables

2.1 Combinations of groups II and VI sources used in MOMBE growth. . 4

2.2 Constants for ZnSe and GaAs for determining the strain in the heterostructure. 15

2.3 Binding energies (meV) of bound excitons in ZnSe [16]. 18

4.1 Known transitions for ZnSe under tensile strain grown on GaAs based on low temperature PL measurements. 26

4.2 Growth conditions for the comparison of the PL for different laser energies. 32

4.3 Growth conditions for the comparison of the PL for the ZnSe grown using DEZn and DESe with different substrate temperatures. 34

4.4 Growth conditions for the comparison of the PL for different Zn fluxes. 37

4.5 Growth conditions for ZnSe grown with DEZn and solid Se. 39

4.6 Growth conditions for the comparison of the PL for the ZnSe grown with solid Zn and DESe sources for different growth temperatures and Zn fluxes. 41

4.7 Growth conditions for the comparison of the PL for the ZnSe grown using DMZn and solid Se sources for different growth temperatures. . 43

4.8 Growth conditions for the comparison of the PL for the ZnSe grown using DMZn and solid Se sources for different DMZn flow rates. . . . 45

4.9 Growth conditions for ZnSe grown using DMZn and DESe. 47

4.10 Growth conditions for the comparison of the PL of ZnSe grown using DMZn and H_2Se for different growth temperatures. 48

4.11 Growth conditions for the comparison of the PL for the ZnSe grown using elemental Zn and elemental Se. 50
4.12 Growth conditions for the comparison of the PL for the ZnSe grown using solid Zn and H_2Se with different substrate temperatures. 55
4.13 Growth conditions for the comparison of the PL for the ZnSe grown using solid Zn and H_2Se with different cracker cell temperatures. . . . 57
4.14 Growth conditions for the comparison of the PL for the ZnSe grown using solid Zn and H_2Se with different Zn fluxes. 59
4.15 Growth conditions for the comparison of the PL for the p-type ZnSe grown by GSMBE with different RF powers. 61
4.16 Growth conditions for the comparison of the PL for the ZnSe:N grown by GSMBE with different N_2 background pressures. 63
4.17 Growth conditions for the comparison of the PL for the ZnSe:Cl grown by GSMBE with different $ZnCl_2$ cell temperatures. 66

Chapter 1

Introduction

Compound semiconductor research is partially directed to the advancement of optoelectronics. Because many compound semiconductors have a direct energy bandgap, it is possible to efficiently achieve light emission from these materials. This, along with the small size of the devices, has led to the use of semiconductor lasers and light emitting diodes in all aspects of electronics and communication systems.

One focus of current optoelectronic research is to achieve semiconductor lasers which emit higher frequencies of light [1] - [4]. An approach to achieve high frequency lasers is through the study of ZnSe, a II-VI compound semiconductor material. ZnSe is a direct bandgap, 2.67 eV at room temperature, semiconductor material. The ZnSe lattice constant of 5.6676 Å is close to that of GaAs, and hence ZnSe can be grown on and integrated with GaAs materials and devices. A laser fabricated with an active region of ZnSe emits blue light, which is one of the highest visible frequencies. The increase in frequency improves some aspects of the communications and the computer industries. For example, implementation of blue lasers with data storage devices, such as a CD ROM (an optical disk drive), allows for a four-fold increase in the density of stored data. More information on the properties of ZnSe in comparison to both Si and GaAs is given in Appendix A.

There are several stages in the development of semiconductor lasers: film growth, characterization, device design, processing, testing and packaging. There are two aspects to the characterization of semiconductor materials, optical and electrical.

This thesis focuses on the optical characterization of epitaxially-grown ZnSe as a function of the growth parameters.

The films are optically characterized using photoluminescence (PL). The measurement is made by optically exciting the sample's surface and collecting the resultant photonic emission, the PL signal. PL is an attractive technique because it is non-destructive. The PL signal is characteristic of the material, showing any defects, impurities or strain that may be present. As a result, every factor in the growth of the material can be analyzed by its effect on the material's optical properties.

In an attempt to optimize the ZnSe film quality and growth rate, several growth parameters have been varied. Different types of sources have been used for the constituent species: metalorganic gases, elemental solids, and gaseous hydrides. The introduction of either a p-type dopant, nitrogen, or a n-type dopant, chlorine, in the ZnSe has also affected the optical properties. Along with these two major studies, the parameter space which includes the substrate temperature and the behavior of the constituent species at the surface has been probed. The effects on the optical quality are examined through a comparison of the photoluminescence of ZnSe grown using different conditions.

The second chapter describes in detail the epitaxial process by which the ZnSe is grown, the growth facilities, and the theory behind the PL measurement. This is followed by a description of the experimental procedure by which a PL measurement and the calibration of the experimental system is made in chapter 3. Chapter 4 shows the PL data for samples grown under various growth conditions with different sources, substrate temperatures and dopants. A discussion follows comparing the PL as a function of these parameters. Finally, the fifth chapter gives a summary of the data and a conclusion, including an outline of future work.

Chapter 2

Background

2.1 Molecular beam epitaxy

A method for compound semiconductor growth is molecular beam epitaxy (MBE). MBE is a process by which beams of molecules or atoms are directed at a heated surface in an ultra high vacuum (UHV) environment forming layers of the compound semiconductor. In MBE, the molecular and atomic beams are formed by heating solid elemental and compound sources.

Such a controlled growth environment has several advantages over other growth techniques, such as metal organic chemical vapor deposition (MOCVD) and organometallic vapor phase epitaxy (OMVPE). The combination of the ultra high vacuum environment and the high purity sources minimizes unintentional contamination. Also monolayer control of the film thickness, alloy composition and doping profiles is possible. Finally, epitaxial growth can be carried out at low growth temperatures which facilitates stoichiometric growth and reduces interdiffusion, such as Ga from the GaAs substrate diffusing into the ZnSe film at the heterointerface.

Group II Source	*Group VI Source*
DEZn	DESe
DEZn	Se
Zn	DESe
DMZn	Se
DMZn	DESe

Table 2.1: Combinations of groups II and VI sources used in MOMBE growth.

2.1.1 Variations on MBE

Two other techniques have been employed in the growth of ZnSe films: metalorganic molecular beam epitaxy (MOMBE) and gas source molecular beam epitaxy (GSMBE). Both growth methods are variations on MBE, where the primary differences are the types of sources used for the constituent species. In both cases, the introduction of new sources leads to a new set of growth parameters required for stoichiometric growth of ZnSe.

Both MOMBE and GSMBE employ at least one gaseous source in the film growth process; a metalorganic and a hydride, respectively. The use of a gas source has the advantage of allowing precise control during growth of the species which has a high vapor pressure in its elemental form, in order to improve the reproducibility of alloy compositions. In MOMBE, several combinations of metalorganic sources and solid sources have been studied [6]. These include diethylzinc (DEZn), diethylselenium (DESe), dimethylzinc (DMZn), solid elemental zinc, and solid elemental selenium (Table 2.1). The metalorganic sources are directed through high temperature cracking cells in order to separate the ethyl or methyl radicals from the constituent elements. One of the disadvantages of MOMBE growth of ZnSe is the apparent blockage of the available surface sites by the ethyl radicals when diethyl-based sources are used. This can affect both the growth rate and the film quality, by reducing the availability of surface sites for the Zn and Se atoms [7, 8].

In GSMBE of ZnSe, a gaseous source, H_2Se, and a solid elemental Zn source are used [9]. The H_2Se is similarly sent through a high temperature cracker before

arriving at the sample's surface. An advantage to GSMBE is that the growth rate is limited by mass transport, whereas in some cases of MOMBE growth, the growth rate is limited due to site blockage by the ethyl radicals. In GSMBE, p-type doping of ZnSe has been accomplished using a nitrogen plasma source [9]. The ability to dope ZnSe p-type is vital for the development of II-VI optoelectronic devices. Until the advent of the nitrogen plasma source, limited success in the p-type doping of ZnSe had been achieved. With this source, nitrogen concentrations as high as $5 \times 10^{18} cm^{-3}$ have been attained [10]. Finally, using GSMBE, n-type doping of ZnSe has been accomplished using a $ZnCl_2$ solid source, where chlorine is the n-type dopant.

2.2 The Physical System

Figure 2-1 shows an overhead view of the chemical beam epitaxy system (CBE) system. CBE employs hydride and metalorganic gas sources for both the Zn and the Se. The CBE system consists of six interconnecting chambers; a transfer chamber, two introduction chambers, a II-VI-dedicated reactor, a III-V-dedicated reactor, and an analytical chamber. Centered in the UHV transfer chamber, a robotic arm allows the samples to be maneuvered between each connecting chamber.

Two separate reactors are used for the growth of the III-V layers and the II-VI layers; a Riber 32P GSMBE system for the growth of III-V compound semiconductors such as GaAs, and a CBE system for the growth of ZnSe and related II-VI compounds. The different families of compound semiconductors are grown in separate systems to avoid cross-contamination during the respective film growth. Each growth chamber maintains an ultra high vacuum (UHV) environment with a base pressure of less than 10^{-9} Torr. Both chambers utilize liquid nitrogen cooled shrouds or traps to minimize the background pressure during growth. A crysoshroud is used in the III-V chamber to thermally isolate the cells, while the II-VI chamber uses water cooling since the cells operate at lower temperatures.

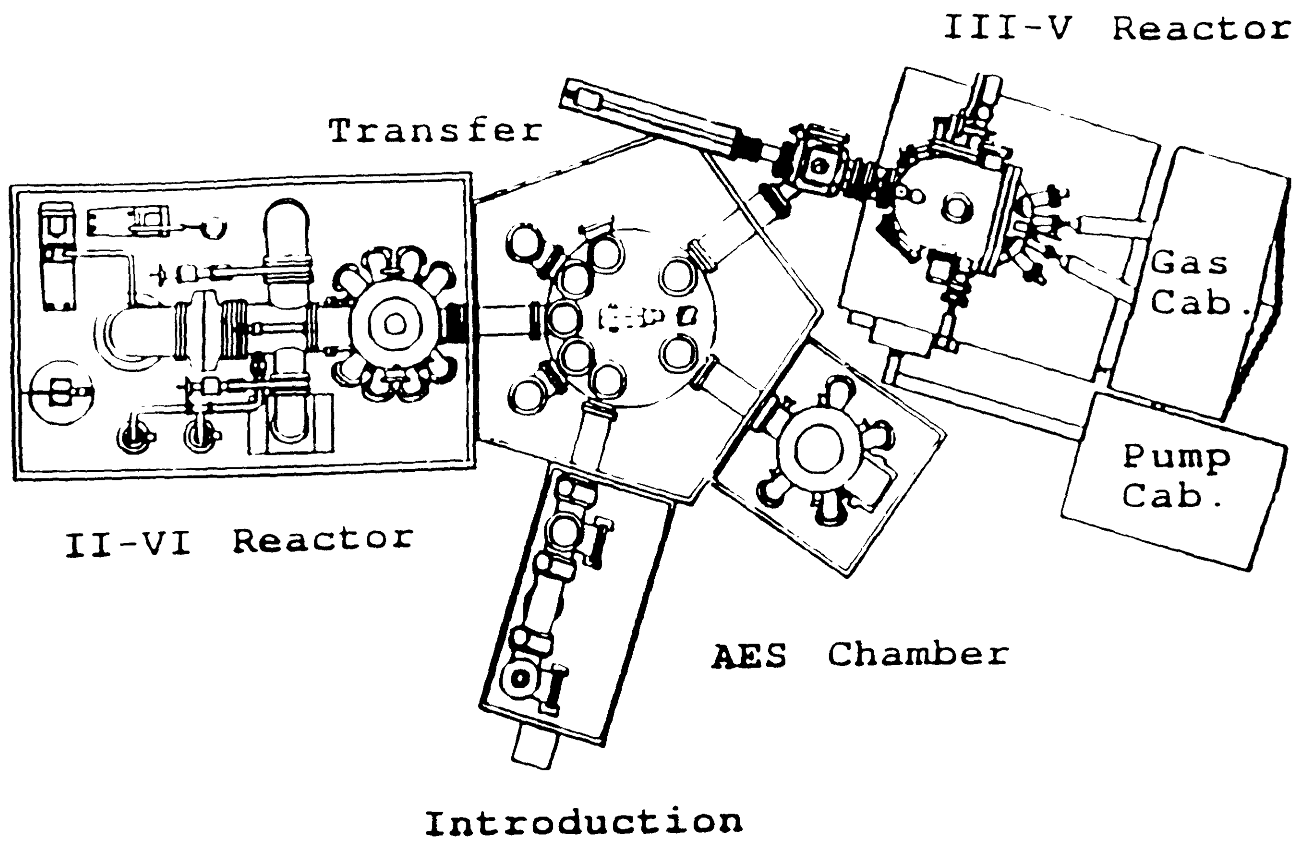

Figure 2-1: An overhead view of the Chemical Beam Epitaxy system.

2.2.1 The Chambers

The introduction chamber for the II-VI reactor consists of two separate vacuum chambers. These two areas share a cryogenic pump allowing only one chamber to be pumped at a time. The first contains a heater and a platform for desorbing the residual acids and water from the surface of a clean sample block prior to mounting a substrate (Appendix B). The second chamber acts as a load lock for the clean substrate and sample block prior to the introduction into the transfer chamber which is connected through a gate valve. From the introduction chamber, the carrier and sample are transported into the transfer chamber using the robotic arm in the transfer chamber. Inside the transfer chamber, a clean sample block with a mounted sample can be baked at another bake station to desorb water.

The III-V chamber is accessed by the buffer chamber. The purpose of the buffer chamber is to allow the II-VI sample blocks to be mated to the III-V sample blocks *in situ*. However, the hardware necessary to perform this action is not available at the present time. Instead, the III-V blocks are loaded directly through the buffer chamber.

2.2.2 The Reactors

After a sample has been baked, it is ready for the ZnSe film growth and can be moved to the reactor. In the II-VI chamber, the sample is suspended by a rotating platform under the substrate heater in the center of the reactor. The substrate heater can be raised and lowered to allow for sample transfers. The elemental sources and the cracking cells are aimed at the substrate. Each source's flux can be interrupted by mechanical shutters. The rate of impingement is estimated by using an ionization gauge or a crystal oscillator prior to growth. The rate of impingement is also measured by reflection high energy electron diffraction (RHEED) intensity oscillations during growth [7]. The substrate temperature is calibrated with a pyrometric evaluation of metal/semiconductor eutectics. The eutectics are thin films of metal deposited on semiconductor substrates which undergo phase transitions at known temperatures.

The phase change in the metal can be detected as a change in the reflectivity. Two different eutectics are currently implemented; Au/Ge, Al/Si, along with the melting point of InSb. The Au/Ge eutectic is used in both II-VI and III-V film growths, because of its low transition temperature, 356°C. The temperatures for the Al/Si eutectic phase transition and the InSb melting point are 577°C and 526°C respectively.

2.2.3 Reflection High Energy Electron Diffraction

The sample is loaded into the reactor and the growth parameters are set. Once the correct growth parameters have been established, the initial surface is prepared by either removing the native oxide or the amorphous capping layer which has been deposited to protect the sample during an *ex situ* transfer between the two reactors. This is accomplished by heating the substrate. The shutters corresponding to the desired sources are then opened in order to allow the fluxes to impinge on the sample's surface. Once the substrate shutter is opened, the respective atoms and molecules are deposited on to the substrate and find their appropriate lattice sites to form a new layer. This layered growth is monitored by observing the Fourier transform of the crystal structure on the reflection high energy electron diffraction (RHEED) screen, a phosphorous-coated glass disc inside the reactor. The RHEED pattern is formed by focusing a 10 keV electron beam at a shallow angle onto the substrate ($< 2°$ from the sample's surface) [11]. The electrons diffract from the substrate surface according to the crystal structure and form a RHEED pattern.

The real time growth rate can be measured using RHEED intensity oscillations [12]. As the molecules are deposited onto the surface there is a periodic nature to the intensity of the RHEED pattern. The reflection is strongest at the beginning of a monolayer and weakest at the half monolayer point, when the surface is roughest. The changes in the surface smoothness during growth can be detected by measuring the intensity of the specular beam with respect to time. The period of the RHEED intensity oscillations corresponds to the time to deposit a monolayer, hence the overall growth rate can be determined.

From the RHEED pattern, it is possible to determine whether the substrate has

a good surface morphology. Also, if the growth is two dimensional, 2D, (layer by layer) RHEED intensity oscillations can be detected. Whereas, if the growth is three dimensional, 3D (islands), RHEED intensity oscillations cannot be detected [12]. Before ZnSe growth, the diffraction pattern of bulk GaAs emerges after the oxide has been removed. At a substrate temperature of approximately 600°C the (2x4) reconstruction appears, which indicates that $\sim$ 75% of the surface sites are covered with As. For the initiation of ZnSe growth, the sources are usually set to achieve a Zn-rich

surface. As the ZnSe nucleation begins, the RHEED pattern changes from a GaAs (2x4) reconstruction to a Se-rich (2x1) reconstruction, and finally to a Zn-rich (2x2) reconstruction. The (2x2) reconstruction is maintained throughout the ZnSe film growth. At the completion of the ZnSe growth, the sources are lowered to their idle temperatures and the substrate heater is lowered to room temperature. The ZnSe film is now ready for analysis and characterization. The exact growth conditions for each ZnSe film will be presented along with its photoluminescence in the Results section, Chapter 4.

2.2.4 Laser-Assisted Growth

During the growth of the ZnSe films, a parallel effort to study the affects of laser-assisted growth was made [7]. A low power laser beam (< 200 mW/cm^2) was directed at the sample surface during the growth of the ZnSe epilayer. The effect of the laser beam on the growth is a function of the sources used. For growth using DEZn and DMZn sources, the laser beam creates photogenerated carriers which effect the species adsorbed on the surface.

2.3 Theory of Photoluminescence

Photoluminescence measurements are based upon two physical principles; optical absorption and optical emission. The first case, optical absorption, takes into consideration the depth at which the PL measurement is capable of probing. The second case,

optical emission, yields information about the energy band structure and impurity concentrations of the sample.

2.3.1 Absorption Coefficient in a Semiconductor

In order to determine the depth over which the PL measurement is probing into a direct-gap semiconductor, the absorption coefficient, α_{abs}, for a semiconductor at a particular pump energy is required. The absorption coefficient determines the change in the optical pump intensity inside the semiconductor as a function of distance (Eq. 2.1) [13];

$$I(z) = I_O e^{-\alpha_{abs} z} \qquad 2.1$$

By definition, α_{abs} is the power removed from the incident beam per unit volume per unit incident flux of electromagnetic energy, and z is the depth into the sample. In order to determine the absorption coefficient for a semiconductor, an understanding of both the incident flux and the probability of transitions from the valence band to the conduction band is required. From the Poynting vector, **S**, the incident flux can be calculated (Eq. 2.2).

$$\mathbf{S} = \frac{c}{8\pi} Re(\mathbf{E}^* \times \mathbf{H}) \qquad 2.2$$

The field vectors, **E** and **H** can be related to the vector potential, **A** by equations 2.3 and 2.4 respectively.

$$\mathbf{E} = \frac{i\omega}{c}\mathbf{A} \qquad 2.3$$

$$\mu\mathbf{H} = \mathbf{\Delta} \times \mathbf{A} \qquad 2.4$$

The vector potential is assumed to be a plane wave of the form:

$$\mathbf{A} = \mathbf{A_o} e^{i(\mathbf{K}\cdot\mathbf{r} - \omega t)} \qquad 2.5$$

Where the propagation constant for the light is denoted by the wave vector, $\mathbf{K}$. Thus, the Poynting vector can be reduced to:

$$\mathbf{S} = \frac{\omega}{8\pi}\frac{\mathbf{n}\omega}{c}|A|^2\mathbf{K} \qquad 2.6$$

where $\mathbf{n}$ is the real part of the complex index of refraction. The magnitude of the Poynting vector is the denominator for the definition for the absorption coefficient.

The numerator for defining the absorption coefficient results from Fermi's Golden Rule:

$$W = \frac{2\pi}{\hbar}|\mathcal{H}_{vc}|^2\rho_{vc}(\hbar\omega) \qquad 2.7$$

where W is the transition probability of electrons going from the conduction band to the valence band per unit time per unit volume, ρ_{vc} is the joint density of states for the conduction and valence bands, and $\mathcal{H}_{vc}$ is the matrix element coupling the valence and conduction bands (Eq. 2.8).

$$\mathcal{H}_{vc} = -\frac{e}{mc}\langle v|\mathbf{A}\cdot\mathbf{p}|c\rangle \qquad 2.8$$

Combining equations 2.6 and 2.8, and writing the joint density of states as;

$$\rho_{vc}(\hbar\omega) = \frac{1}{2\pi^2(\frac{2m_r}{\hbar})^{3/2}\sqrt{\hbar\omega - E_g}} \qquad 2.9$$

where m_r is the reduced mass for the valence and conduction bands, the frequency dependence of the absorption coefficient is:

$$\alpha_{abs} \propto \frac{A}{\hbar\omega}\sqrt{\hbar\omega - E_g} \qquad 2.10$$

where A is a constant dependent on the particular material system being studied and E_g is the material's energy gap. Therefore, for a known optical energy, the decay of the intensity as a function of the depth into the sample can be determined. The absorption of light corresponding to the laser wavelength used in the ZnSe photoluminescence experiments is shown in Figure 2-2. This approach does not take into consideration

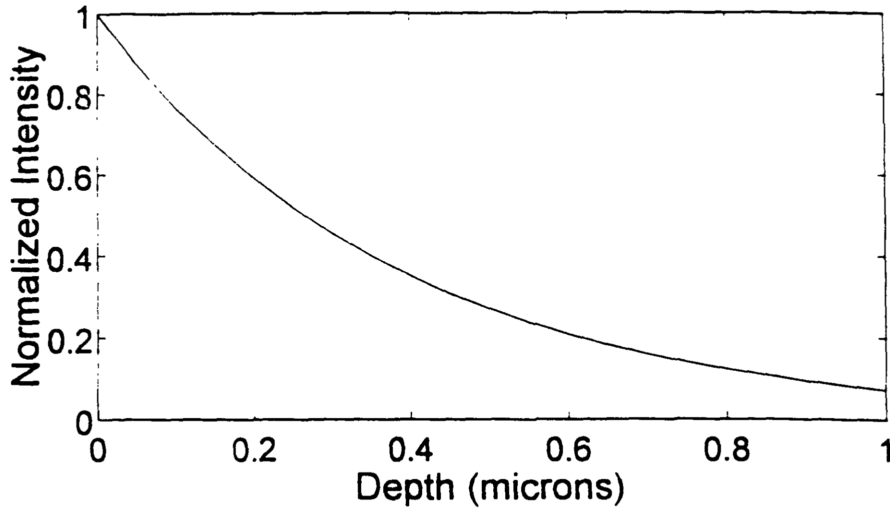

Figure 2-2: The absorption of photons corresponding to the wavelength of the laser used in the PL experiment (3250 Å) as a function of depth into the ZnSe.

the effects of generated photons on the rest of the sample. For example, a photon that is generated in the ZnSe layer may reach the III-V buffer layer if it is not absorbed back into the ZnSe layer. Because the energy associated with a photon emitted from the ZnSe layer is generally larger than the energy gap of the III-V layer, a recursive effect can result, where the luminescence from the ZnSe can cause luminescence from the III-V layer. Since the emission from the III-V layer will have an energy less than the band-gap energy of ZnSe, the photon will, ideally, reach the sample's surface and be emitted.

2.3.2 Energy Bands in Semiconductors

In the previous section, a direct gap semiconductor was assumed. This is an important characteristic of optical semiconductor materials. Direct gap semiconductors have a maximum in the valence band and minimum in the conduction band at simultaneous points in momentum space, or k-space (Figure 2-3). The minimum energy gap generally occurs at k=0, and will be the case henceforth. As a result, optical transitions do not involve a translation in momentum space. Hence, any emission measured from a direct gap semiconductor is directly related to the energy band structure at k=0.

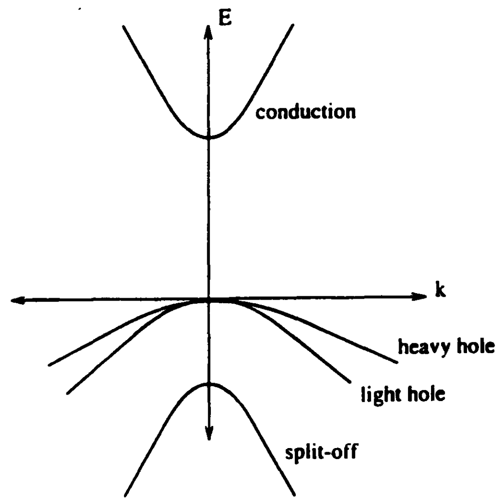

Figure 2-3: The energy band structure for a direct gap semiconductor such as ZnSe.

There are several energy bands in an ideal semiconductor which can be probed with PL. In the valence band, there are three bands; the light hole (lh), the heavy hole (hh), and the split-off bands. The lh and hh bands are degenerate at k=0, and the split-off band is slightly lower in energy than the other two. The energy separation between the valence band and the conduction band at k=0 in a direct gap semiconductor is the energy gap, E_g. For ZnSe, the room temperature band gap energy is 2.67 eV. The valence band is full of electrons at equilibrium, and, across the energy gap, the conduction band is devoid of electrons. When a semiconductor is heated or externally pumped (optically or electronically), electrons are excited to the conduction band. The electrons then decay back to a lower energy level in the valence band. As the electrons fall in energy, conservation of energy dictates that the energy loss must be found elsewhere in the system. Ideally, in a PL measurement, the energy loss results in photon emission. In the PL measurements, the energy of the optical excitation exceeds the bandgap energy. As a result, electrons can be pumped across the band gap to the conduction band, or to higher levels within the conduction band. Often, the higher energy levels are not detected with the PL measurement, because the decay of the electrons from these higher states is complicated by intermediate steps at the conduction band.

2.3.3 Strain in Heterostructures

Heterostructures often have the added factor of strain resulting from lattice mismatch between the different material systems. Strain in a material may be manifested as biaxial tension or compression. The thickness of the epitaxial layer and the degree of lattice mismatch determine how the strain affects the heterostructure. Relaxation of the elastic strain results in the formation of interfacial dislocations. The interfacial dislocations begin to form at a critical epitaxial layer thickness, h_c, when it is energetically favorable to form dislocations rather than elastically deforming the lattice. For thin epilayers, the entire epilayer is strained to match the lattice constant of the substrate.

The degeneracy in the lh and hh valence bands at k=0 is split when the heterostructure is strained. For compressive strain, the heavy hole band has a higher energy than the light hole energy band. Also, the resulting bandgap is larger than the unstrained bandgap. The reverse is true for tensile strain. Strain in the epitaxial layer is calculated from Eq. 2.11

$$\varepsilon = \frac{(a_f - a)}{a} \qquad 2.11$$

where a_f and a are the lattice constants of the epilayer and the substrate, respectively [14].

For a layer under compressive strain, the bandgap energy increases according to equation 2.12.

$$+\Delta E_G(\varepsilon) = 2a_G(C_{11} - C_{12}/C_{11})\varepsilon - b(C_{11} + 2C_{12}/C_{11})\varepsilon \qquad 2.12$$

Similarly, for a layer under tension, the decrease in bandgap energy is,

$$-\Delta E_G(\varepsilon) = 2a_G(C_{11} - C_{12}/C_{11})\varepsilon + b(C_{11} + 2C_{12}/C_{11})\varepsilon \qquad 2.13$$

where C_{11}, C_{12} are elastic constants, b is the valence band deformation potential, and a_G is the hydrostatic deformation potential.

Constant	*GaAs*	*ZnSe*	*Ref*
Lattice constant a, (Å)	5.6533	5.6676	[15, 16]
Elastic constant C_{11} ($10^6 kg/cm^2$)	12.1	0.826	[15, 17]
Elastic constant C_{12} ($10^6 kg/cm^2$	5.48	0.498	[15, 17]
Valence band deformation potential, b (eV)	-1.7	-0.4	[15, 18]
Hydrostatic deformation potential a_G (eV)	2.7	-4.25	[15, 18]
Thermal expansion coefficient ($\frac{1}{°C}$)	6.4x10^{-6}	9.44x10^{-6}	[15, 16]

Table 2.2: Constants for ZnSe and GaAs for determining the strain in the heterostructure.

Table 2.2 lists some of the constants which are used to determine the strain between GaAs and ZnSe [15] - [18]. For ZnSe grown on GaAs, there is a 0.25% lattice mismatch at room temperature at the interface. As a result, a thin film of ZnSe is compressively strained to match the GaAs lattice constant. The bandgap energy of the ZnSe film increases by $\sim$ 6meV, as calculated using the constants in Table 2.2 [19]. For a thicker film, $>$ 1500Å, the ZnSe relaxes, creating interfacial dislocations, which lowers the residual strain in the film.

Because the thermal expansion coefficients of the ZnSe and the GaAs are different, a thermal strain manifested by biaxial tension occurs when the heterostructure is cooled to 10 K for photoluminescence measurements. The tensile strain is around 0.04 % and hence, decreases the bandgap energy by $\sim$ 2 meV [15]. A plot of the change in the bandgap energy as a function of strain for a ZnSe layer grown on GaAs is shown in Figure 2-4. For thick ZnSe films that are relaxed, the tensile strain pushes the light hole energy band above the heavy hole energy band. As a result, the PL features which involve the valence band will correspond to transitions from conduction band or donor states to the light hole band. For thin films, ($<$ 1500Å), the compressive strain pushes the heavy hole energy band above the light hole energy

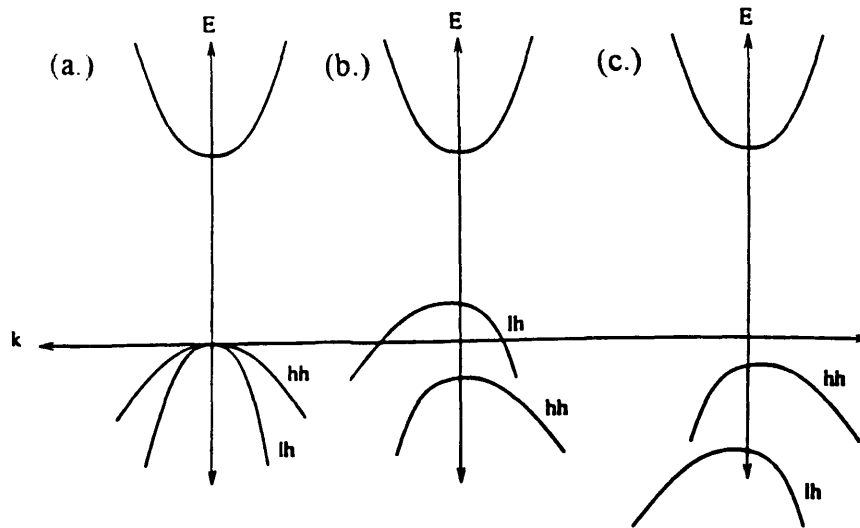

Figure 2-4: The manifestation of strain in a direct gap semiconductor such as ZnSe; (a) unstrained, (b) biaxial tension, (c) biaxial compression.

band. Hence, the dominant PL features will correspond to transitions involving the heavy hole band.

2.4 Impurities, Excitons, Phonons

In an imperfect compound semiconductor material, impurities create additional energy states inside the band-gap. For an impurity which donates an electron to the lattice, there is a donor energy band, at an energy E_D with respect to the valence band. Similarly, an electron-accepting impurity creates an acceptor energy band, at an energy E_A with respect to the valence band, (Figure 2-5(a)). The exact energies corresponding to transitions from either impurity band is a function of the ionization energy of the respective impurity.

An electron transition can occur from a donor band to the valence band, or from the conduction band to an acceptor band (Figure 2-5(a)). The transition probability for either occurrence can be found by assuming that the impurity energy levels tend to be shallow, discrete, and nonoverlapping [20]. For the donor to valence band transition, at k=0, the transition rate is:

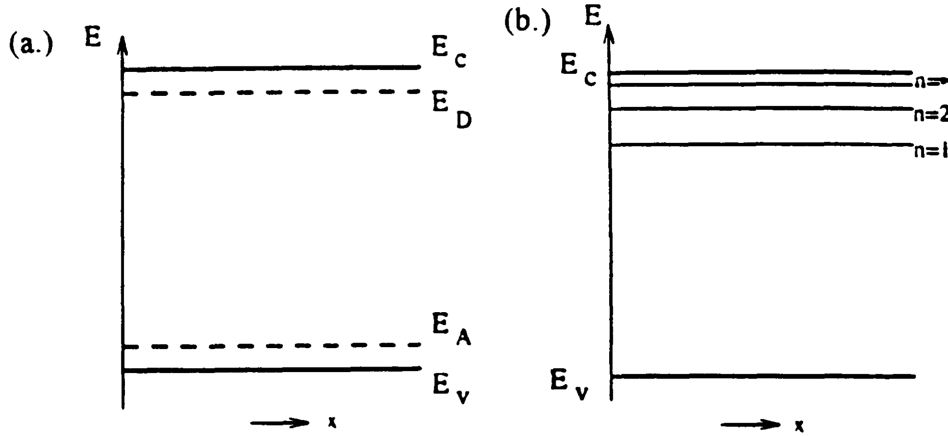

Figure 2-5: The energy band structure at k=0 for (a) impurities and (b) free excitons.

$$\frac{1}{\tau_{p_o}} = 64\sqrt{2}\pi \mathbf{n} \frac{q^2\hbar^2\omega|P_{vc}|^2}{c^3m^2(m_cE_D)^{3/2}} n_D \qquad 2.14$$

where, $|\mathbf{P_{vc}}|$ is the averaged interband-matrix element of the momentum operator, E_D is the impurity ionization energy, n_D is the density of electrons in the donor band, m_c is the effective mass of the conduction band electron, and **n** is the index of refraction [20]. The transition rate for the conduction band to acceptor, at k=0, is:

$$\frac{1}{\tau_{n_o}} = 64\sqrt{2}\pi \mathbf{n} \frac{q^2\hbar^2\omega|P_{vc}|^2}{c^3m^2(m_AE_A)^{3/2}} p_A \qquad 2.15$$

where, p_A is the density of holes in the acceptor band, E_A is the ionization energy of the impurity, and m_A is the effective mass of holes.

The energy band structure at k=0 is further complicated by the presence of free excitons. A free exciton is an electron-hole pair with stable bound states resulting from Coulomb attraction. The energy of the pair is less than the bandgap energy. In the band structure, the exciton adds a set of energy levels close to the bottom of the conduction band (Figure 2-5(b)). For the majority of compound semiconductors, the exciton is ionized at very low temperatures, and, hence, does not contribute to the PL spectra. The ZnSe system is more ionic than III-V materials, and therefore, the

Donor	E_d	E_{BX} *neutral*	E_{BX} *ionized*
Al	26.3	3.96	5.35
Cl	26.9	4.05	5.76
Ga	27.9	4.3	7.62
In	28.9	4.5	7.62
Na	90-128	8.5	

Table 2.3: Binding energies (meV) of bound excitons in ZnSe [16].

excitonic structures are intact at 10° K (the measurement temperature). The free exciton energies in ZnSe are 21 meV and 25.7 meV corresponding to holes from the light and heavy hole bands, respectively [21, 22].

With the presence of impurities, bound excitons arise. When bound excitons recombine, the emission has a slightly lower energy than the energy of a free exciton. A free hole can combine with a neutral donor to form a donor-bound exciton, where the electron bound to the donor interacts with the hole. Similarly, a free electron can combine with a neutral acceptor to form an acceptor-bound exciton. The energies of both excitons upon recombination are close to the bandgap energy. Table 2.3 lists the binding energies, E_{BX}, of some donors in ZnSe [23]. The binding energy is the energy required to separate an exciton from an impurity.

Other sources of radiative emission are the longitudinal optical (LO) and transverse optical (TO) phonons. In a direct transition, the phonon emission results from an excited electron relaxing to a position corresponding to a minimum potential in the conduction band. The relaxation involves both an energy loss as well as a change in momentum, which are compensated by the emission of an optical phonon. The signature of the radiation of optical phonons is a number of equally separated features (with respect to energy) decreasing in intensity. The LO phonon occurs more often in the PL of ZnSe, with an energy separation of 31.9 meV [24].

Chapter 3

Experimental

3.1 Photoluminescence Set-Up

In this study, the experimental set-up for the photoluminescence measurement is divided into four subsystems; temperature control, optical pumping, optical detection, and data acquisition (Figure 3-1). The first of these, temperature control, consists of a closed-cycle compressed helium Janis cryostat. The cryostat is evacuated to less than 10^{-4} Torr with a combination of a mechanical roughing pump and a molecular drag pump. The cryostat is capable of maintaining a stable temperature of 10 K. Several samples are simultaneously mounted inside the cryostat on the cold finger. The sample temperature is monitored and controlled from 10 K to 300 K using a silicon diode attached to the base of the cold finger.

Simultaneously mounting multiple samples has several advantages. Not only is the experiment less time-consuming, the conditions under which the PL data is taken are assuredly the same for each sample. This allows for a more accurate comparison of the energies of the PL features, especially when the measurements are taken over a range of temperatures. Also, it is possible to mount a sample with an area of 1 cm^2, to study the uniformity of the optical properties across the sample.

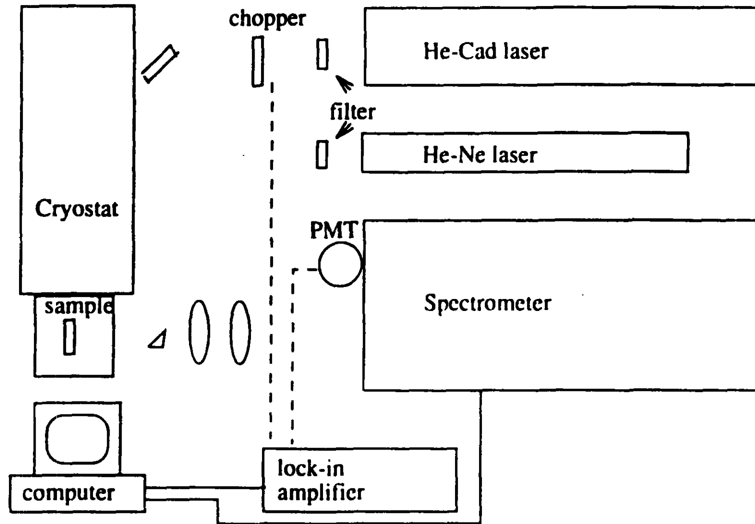

Figure 3-1: The photoluminescence set-up.

3.1.1 Optical Pumping

The sample is optically pumped by a laser beam, from either a 325 nm He-Cd laser (for II-VI and large band gap III-V materials) or a 632.8 nm He-Ne laser (for narrow band gap III-V materials), where the laser emission energy is larger than the band gap energy of the material. The power density can be varied from a few mW/cm^2 to a few W/cm^2 by changing the laser spot diameter on the sample's surface, as well as the laser power using neutral density filters. Both lasers are similar in power ($\sim$ 8 mW), but the He-Ne laser has a slightly larger spot size than the He-Cd laser.

Both lasers travel similar paths to the sample. The beam is sent through a laser line interference filter which passes only the primary laser line. Then, the beam passes through an optical chopper and is focused with a lens onto the sample's surface. The final laser power at the sample surface is around 0.45 mW, and the spot diameter is around 300 μm, corresponding to a power density of 0.64 W/cm^2. The large power loss occurs mainly at the interference filter, which transmits about 25% of the primary

laser line. The laser is optically chopped to create a modulated signal at the sample surface. As a result, it is possible to differentiate between the PL signal and any spurious noise at the data acquisition stage.

3.1.2 Optical Detection

The optical detection stage consists of two lenses, a Hamamatsu photomultiplier tube, and a 1/2 meter Jarrell Ash spectrometer. The luminescence from the sample surface is collected using two lenses. The first lens collects and collimates the luminescence from the sample. The second lens focuses the luminescence onto the slits of the spectrometer. The spectrometer is scanned over a range of wavelengths. As the spectrometer passes a wavelength corresponding to the luminescence, the light leaves the spectrometer at a second set of slits. A photomultiplier tube detects and amplifies this light with a gain of up to 10^6. The wavelength calibration of the spectrometer is made by collecting a second harmonic laser line from the He-Cd laser at 6500 Å.

3.1.3 Data Acquisition

The signal from the photomultiplier tube and the corresponding wavelength setting of the spectrometer are collected in the data acquisition stage. This stage is primarily a lock-in amplifier, a preamplifier, and a computer. The frequency of the optical chopper is sent to the lock-in amplifier, along with the signal from the photomultiplier tube (which has been first sent through a preamplifier-amplifier). For a given time constant, the lock-in demodulates the signal from the photomultiplier tube and sends the average to the output and eventually, to the computer. This reduces the level of background noise, and allows for the detection of signals as small as 1 μV. The analog output of the lock-in amplifier is digitized by a computer equipped with an analog-to-digital converter. The data over a given range of wavelengths is analyzed with the aide of computer software [25].

The resulting PL spectra is an indication of the optical quality of the material. Changes in the PL parameters (measurement temperature and excitation power den-

sity) can be used to study different effects in the PL.

3.2 System Calibration

A number of measurements were made to optimize the PL system. First, the effect of changing the excitation power density was examined. The power was changed by inserting neutral density filters in the path of the laser prior to the sample. Figure 3-2 shows a set of PL spectra for a sample pumped by different power densities, varying from 640 mW/cm^2 to 6.4 mW/cm^2. Both of the full-width at half maximums (FWHMs) and the energies of the peaks are similar regardless of power density. The PL resulting from lower power densities has better resolution for closely spaced peaks, but it is also plagued by background noise. For weakly emitting samples, such as samples dominated by free excitons, a higher power density is necessary to increase the signal to noise ratio to a useful level. Also higher power densities can saturate some defect band features such that they might not appear in the PL at various intensity levels.

Due to the large bandwidth of interest, 1.2 eV, the problem of chromatic aberration arises. The collection lenses have different focal lengths for different wavelengths of light. As a result, finding the relative intensity of the features is complicated by the requirement that the lenses be realigned within the scan range. In general, for ZnSe samples dominated by a large defect band (in the yellow to orange range of emission), the collection lenses are aligned to optimize for the wavelengths corresponding to the defect band for a wide bandwidth scan. A narrow bandwidth scan is taken over the energy range corresponding to band-edge energies, with the lenses aligned to optimize the band-edge features. For samples which show no visible defect band, the alignment is centered on the band-edge features.

Finally, to have a general idea about the optical properties of ZnSe grown on a III-V substrate, it is essential to understand the optical properties of pure ZnSe. Figure 3-3 shows the PL from a ZnSe bulk crystal. The primary feature with an energy of 2.779 eV, corresponding to an exciton bound to a Zn vacancy, and a FWHM of 2.4

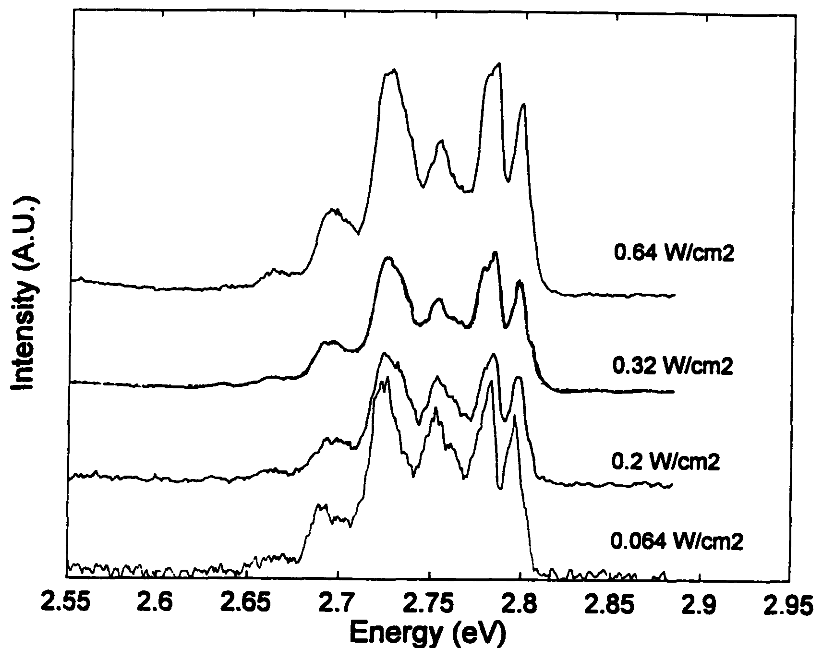

Figure 3-2: The PL of a ZnSe film at several different laser excitation power densities.

meV indicates the resolution limitations of the PL system. The other features to the left of the primary feature correspond to LO phonon replicas of the exciton transition. Excitonic PL features in ZnSe at low temperatures are often accompanied by phonon replicas, for momentum conservation. The longitudinal optical phonon replicas, LO phonons, are separated by 31.9 meV [24]. The two features to the right of the bound exciton feature at 2.779 eV correspond to a donor-bound exciton at 2.794 eV, and a free exciton at 2.801 eV. The donor-bound exciton results from impurities in the lattice. PL can be used, when supplemented by other characterization methods, to determine the respective impurities.

3.3 System Limitations

The spectrometer has a resolution limitation on the order of 8 Å, or 4 meV at energies near 2.7 eV and 3 meV at energies near 2.4 eV when the slit width used is 50 μm. For a higher resolution system (with a 1 meter spectrometer), the FWHM for the same

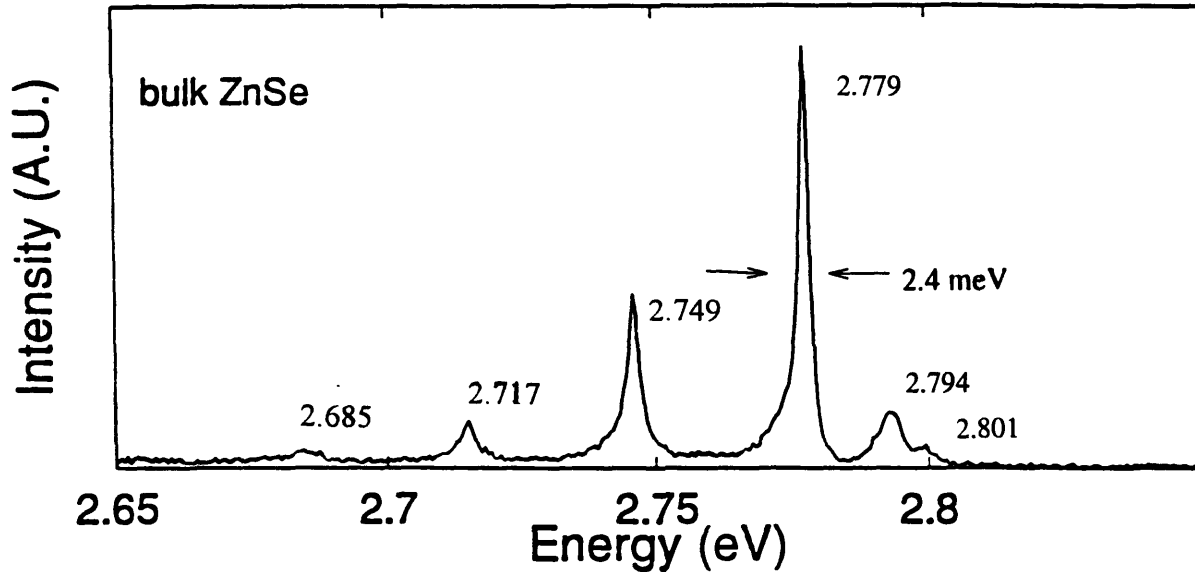

Figure 3-3: The PL of a bulk-grown ZnSe sample showing feature energies and the FWHM realizable for the experimental apparatus.

feature has been reported to be as small as 0.3 meV [14]. However, the spectrometer in the PL system has an optimal resolution of 2 Å, or 0.6 meV, for narrower slit widths. Closing the slits further reduces the collected luminescence to the extent that the noise in the detection and acquisition electronics exceed and distort the PL signal. Hence, a compromise between resolution and signal level is maintained with a less than optimum slit width.

Chapter 4

Results and Discussion

The PL spectra of ZnSe films grown on GaAs substrates using different sources of Zn and Se are presented in this chapter. There is an abundance of literature on the optical properties of MBE-grown ZnSe based upon PL measurements [14, 15, 24, 26, 27, 28]. As a result, the origin of the features generally seen in PL are well-defined. However, the optical properties of ZnSe grown by GSMBE, MOMBE, and CBE have not been thoroughly investigated. Table 4.1 shows the 4.2 K energies and the corresponding explanations for the PL features for thick ($> 2\mu m$), MBE-grown ZnSe films under tensile strain due to the PL measurement temperature [14, 24, 29]. The self-activated emission band (SA) is attributed to donor-acceptor pair transitions involving shallow donors, the occurrence of zinc vacancies, and the resulting Se complexes [29]. The neutral donor-bound exciton transitions, 2.792 eV and 2.797 eV, correspond to the presence of carbon and chlorine impurities, respectively in the ZnSe [24, 26].

Although the origin of the PL features of ZnSe are understood, the energies at which the respective peaks occur are strongly dependent upon the growth parameters and the sources, as well as the measurement parameters. The effects of these parameters on the PL are understood, and can be identified. For example, the heavy hole (hh) free exciton feature decreases both in energy and FWHM as the film thickness increases. The trends in the energy and the FWHM of the hh free exciton feature have been measured by photoreflectance and are shown in Figure 4-1 [27].

A similar trend exists for variations in the growth temperature [14]. For an in-

Name	*Energy (eV)*	*Explanation*	*Ref.*
Ex^1	2.8020	Free exciton, hh	[15]
Ex^2	2.8000	Free exciton, lh	[15]
I_1	2.790	Neutral acceptor-bound exciton	[14]
$I_1{}^{deep}$	2.782	Deep acceptor-bound exciton	[14]
I_2	2.797	Neutral donor-bound exciton, chlorine	[24]
I_2	2.792	Neutral donor-bound exciton, carbon	[26]
I_3	2.7958	Ionized donor-bound exciton	[24]
Y_0	2.60	Due to extended defects	[28]
SA	2.386	Defect band	[29]

Table 4.1: Known transitions for ZnSe under tensile strain grown on GaAs based on low temperature PL measurements.

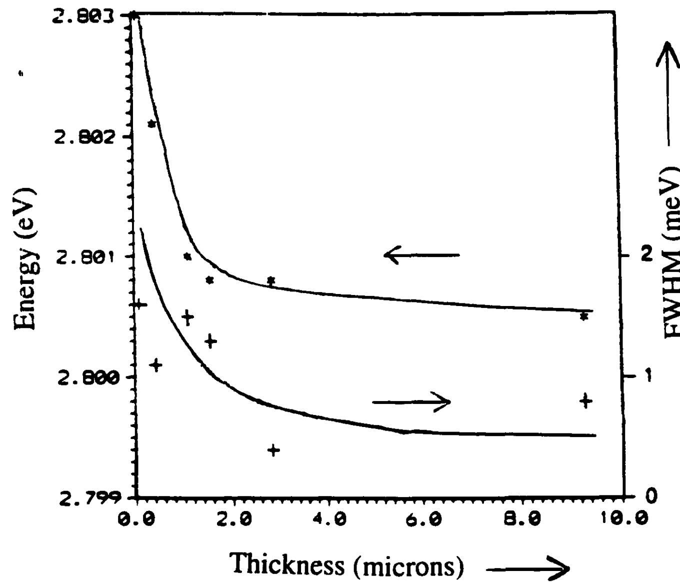

Figure 4-1: Photoreflection of ZnSe epilayers at T=10 K. Thickness dependence of the resonance energy and the half-width of the heavy hole exciton [27].

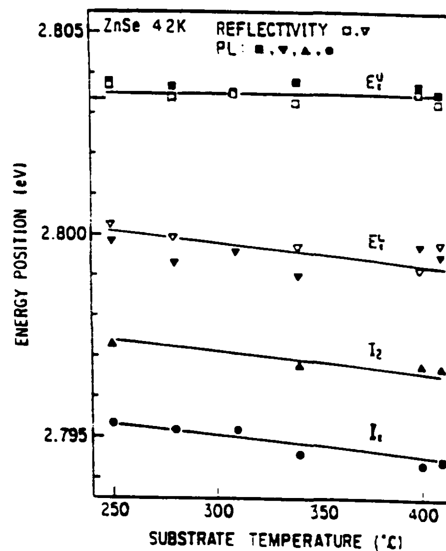

Figure 4-2: The peak position of bound exciton emission lines and free exciton as a function of the substrate temperature [14].

creasing substrate temperature, T_{sub}, a downward shift in the feature energies for the light hole (lh) free exciton, the neutral acceptor-bound exciton and the neutral donor-bound exciton transitions occurs due to thermal stress between the ZnSe and the GaAs [14]. Since ZnSe and GaAs have different thermal expansion coefficients, a thermal stress results, creating a 2D tensile stress in the ZnSe. Hence, increasing the substrate temperature during growth increases the thermal stress (or 2D tensile stress at 4.2 K) and causes the ZnSe energy bands to shift, altering the PL. This is shown in Figure 4-2 [14]. However, the hh free exciton transition remains constant in energy with T_{sub} as seen in Figure 4-2 after reference [14]. For thin films ($< 1\mu$m), the dominant free exciton transition is a heavy hole free exciton, whereas for thicker films, the light hole free exciton is dominant. Compressive strain is associated with a "heavy hole up" condition, and tensile strain with a "light hole up"condition, hence the strain of a ZnSe film can be determined by the free exciton transition energies.

4.1 MOMBE Growth

Several combinations of metal-organic and solid sources have been employed to optimize the growth of ZnSe. The bulk of the effort was to obtain a growth rate

comparable to MBE ($\sim 1\ \mu$m/hr) while employing gas sources. A parallel effort analyzing the effects of laser illumination during growth has resulted in a variation in the properties of each sample across its surface. An example of the PL of a MOMBE sample at several points on the surface from a thin region (1000 Å) which did not have laser-assisted growth, to a thicker region (1800 Å) which had laser-assisted growth (Figure 4-3) shows the variation in the optical properties with respect to laser-assisted growth. The donor-bound exciton feature of each scan is labelled by a symbol. The PL scan with an '*' labelling the donor-bound exciton feature corresponds to the thinnest region, with no laser-illumination during growth. The other scans correspond to progressively thicker regions of the sample, where increasing power densities of laser-illumination occurred during the growth. The PL shows changes in the relative intensities of the features with respect to the regions of increasing thickness. As the thickness increases (and, hence, the power density of the laser-illumination increases), the donor-bound exciton feature increases in intensity with respect to both the donor-acceptor pair (DAP) and the defect band ($\sim$ 2.3 eV) features. The increase in the intensity of the donor-bound exciton indicates a higher degree of stoichiometry in the film.

This section is subdivided into three main subsections according to the sources employed during the growth of ZnSe. The first main subsection compares the PL from ZnSe grown using DEZn and DESe sources. Within this subsection, the PL for variations in substrate temperature, laser illumination energy, and Zn flux is presented. The second subsection deals with the PL from ZnSe grown with one diethyl-based source and one elemental source. Each combination is dealt with separately. Finally, the last subsection presents the PL for ZnSe grown with one dimethyl-based source with variations in the growth parameters and the sources.

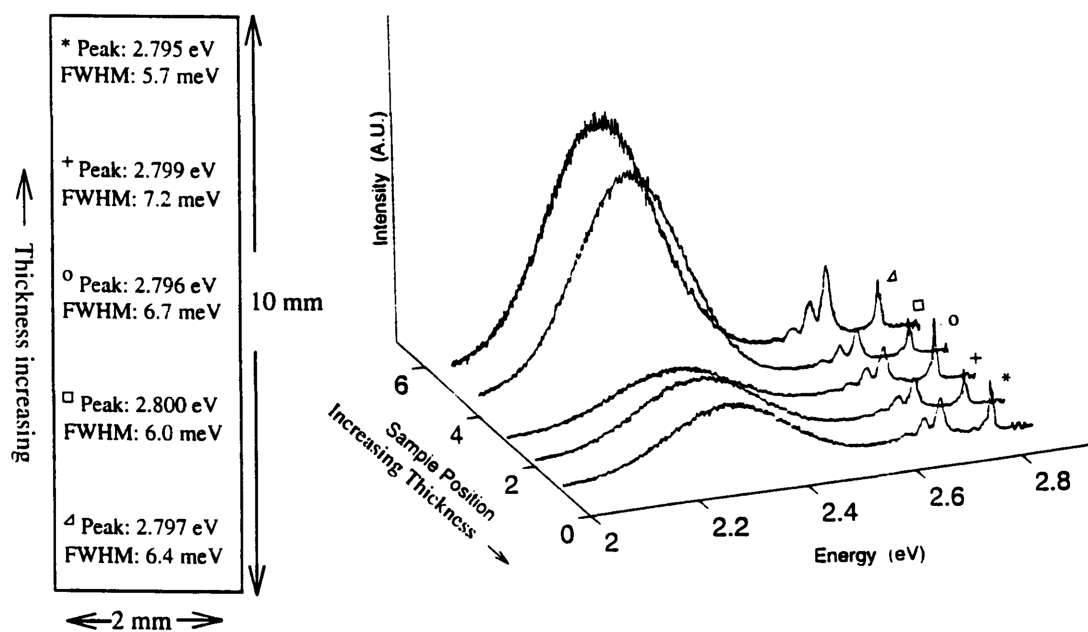

Figure 4-3: PL of ZnSe grown by MOMBE at several points on the sample surface.

4.1.1 ZnSe Growth with DEZn and DESe Sources

Three comparisons are made of the PL of ZnSe grown using DeZn and DESe as sources. In order to understand the mechanism by which photo-assistance affects the growth of ZnSe, the PL of ZnSe grown using different laser illumination energies is first considered. Next, three ZnSe films grown at different substrate temperatures are compared. The third comparison is for variations in the Zn flux during ZnSe growth.

Different laser illumination energies were used during ZnSe film growth while holding the other growth parameters constant (Table 4.2). The enhancement ratio, i.e. the ratio of the thicknesses of the illuminated region to the unilluminated region, increases with increasing laser energy, with a critical point at the bandgap energy [8]. The enhancement ratios for these growths are shown Figure 4-4. For laser illumination energies above or near the bandgap energy, the enhancement ratio is ~ 3 for the growth conditions employed. The PL for these samples (Figure 4-5) shows an improvement in the relative intensities between the defect band and the bandedge features when the laser, that is used to illuminate the surface during growth, has an energy greater than or equal to the energy of the interband impurity states. The PL of the different samples are labelled according to the growth number and whether or not the region is laser illuminated, where 'nl' indicates no laser illumination and 'l' for laser illumination. The intensity scale is not normalized unless otherwise stated. All of the films grown without laser illumination are pseudomorphic with the GaAs substrate, and thus have the same lattice constant as GaAs. Hence, the combination of the strain due to the lattice mismatch as well as the slight variation in growth temperatures results in different energies for the band-edge features.

The films that are grown with laser assistance using laser emission wavelengths of 4579 Å and 4880 Å (Figures 4-5 (d)-(g)) have more prominent bandedge features; a donor bound exciton (2.796 eV) and a DAP (2.737 eV). Both of these illumination energies, along with the illumination energy of growth # 53 (Figures 4-5 (b) and (c)), are less than the ZnSe band-gap energy, but are within range of the interband defect state energies. Growth # 46 (Figures 4-5 (h) and (i)) was illuminated with a laser with an emission energy greater than the bandgap energy; whereas growth # 57

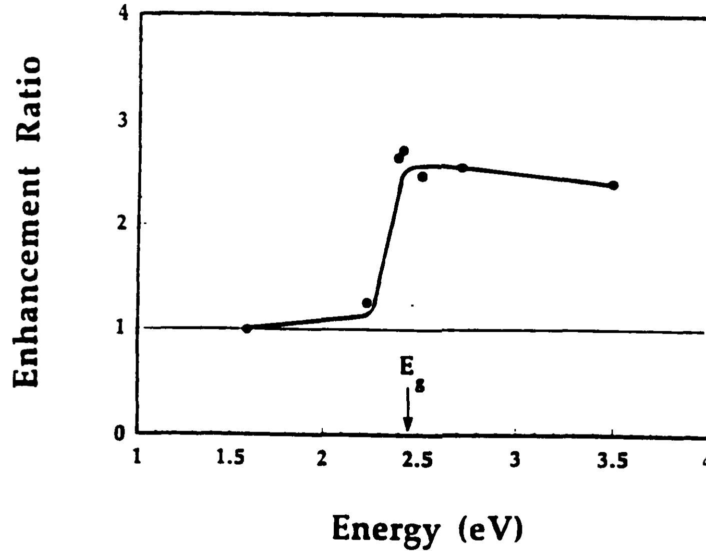

Figure 4-4: Enhancement ratio for ZnSe grown using DEZn and DESe with different laser illumination energies. The line is drawn to aid the eye. The arrow denotes the bandgap energy at growth temperatures [7].

(Figure 4-5 (a)) was illuminated with a laser with an emission energy less than the ZnSe bandgap energy. Also the intensity of the neutral donor-bound energy increases in the illuminated regions, as compared to the unilluminated regions.

The trends in the PL cannot be entirely associated with the laser illumination energy. Growth # 57 is thinner than the other samples, and all of the samples' unilluminated regions are below the critical thickness and should be pseudomorphic to the GaAs substrate. Also, the growth temperature is slightly lower in growth # 46. The presence of the laser definitely affects the relative intensities between the defect band and the bandedge features, as well as between the different bandedge features.

From these comparisons, it is clear that the effect of above bandgap illumination is to improve the stoichiometry of the ZnSe. The improvement is demonstrated by the occurrence of luminescence originating from near bandedge.

ZnSe Growth #	*46*	*44*	*42*	*53*	*57*
Growth Time (Hr)	4	4	4	4	4
T_{sub} (^oC)	340	355	355	360	355
Cracker T_{Se} (^oC)	800	800	800	800	800
Cracker T_{Zn} (^oC)	50	50	50	50	50
DESe flow rate (sccm)	0.5	0.5	0.5	0.5	0.5
DEZn flow rate (sccm)	0.5	0.5	0.5	0.5	0.5
Laser λ Å	3511-3638	4579	4880	5145	7800
Unilluminated thickness Å	1350	1250	1250	1100	850
Illuminated thickness Å	3200	3300	3350	3000	850

Table 4.2: Growth conditions for the comparison of the PL for different laser energies.

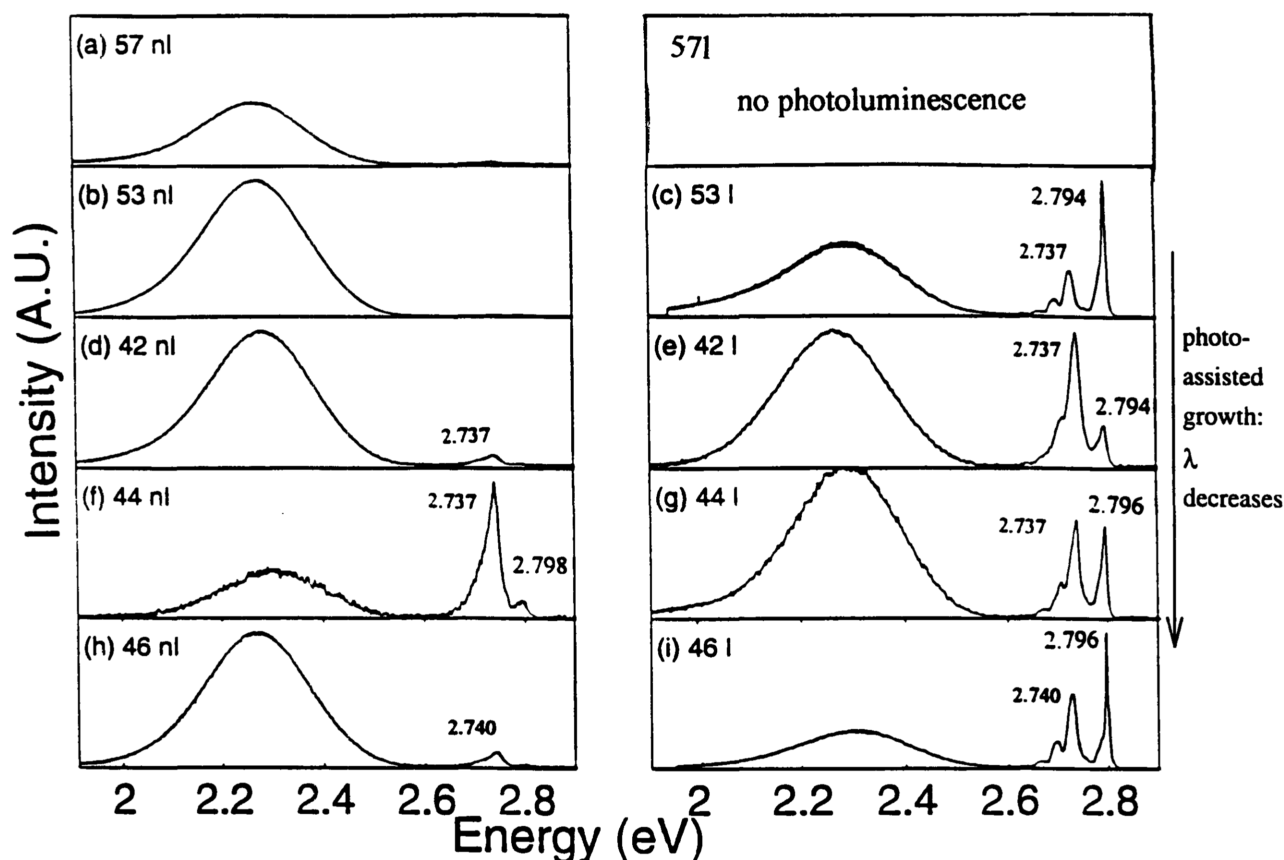

Figure 4-5: PL of ZnSe grown using DEZn and DESe with different laser illumination energies. (a) 7800 Å, (b) and (c) 5145 Å, (d) and (e) 4880 Å, (f) and (g) 4579 Å, (h) and (i) 3511-3638 Å. The intensities were not normalized.

Variations in Substrate Temperature

The PL spectra for three ZnSe samples grown using similar conditions, with different substrate temperatures (Table 4.3) are shown in Figure 4-6. The film thicknesses for the three samples, ranges from 700 to 9200 Å, with the laser illuminated regions being the thickest. The enhancement ratio, the ratio of the illuminated and the unilluminated thicknesses, is larger than unity in all three cases, but decreases with increasing substrate temperature. Also, all of the unilluminated regions, along with the illuminated region of growth # 51, are significantly thinner than the critical thickness (1500 Å), resulting in PL features with varying energies.

Figure 4-6(a) shows the PL for the thickest sample (growth # 50 with laser illumination). The unilluminated area of growth # 50 was polycrystalline (as determined by RHEED during growth); hence there were no detectable PL features. At a growth temperature of 250°C, the DEZn is not efficiently pyrolyzed, and the resultant film is therefore highly nonstoichiometric. Growth # 50 is speculated to be primarily composed of Se, and thus does not luminesce. The presence of a strong PL signal from the illuminated region indicates that during growth the laser illumination has increased the supply of Zn to the sample surface, through the generation of carriers which break up the ethyl radicals. Although the relative intensities of the defect band and the bandedge features favor the bandedge features, the primary bandedge feature is a neutral donor-bound exciton, I_2 at 2.794 eV. Since the film is so thick (9200 Å), there is no way of determining the nature of the defects at the heterointerface using PL beyond considering the low intensity of the defect band. To the right of I_2, there is a small feature corresponding to a free exciton (at 2.802 eV), indicating high crystalline quality. The I_2 feature is very wide (FWHM = 22 meV), which indicates that there is more than one transition within the feature.

For a film which is one third as thick as growth # 50, Figure 4-6(c), the laser-assisted portion of growth # 28 has a much larger defect band in relation to the bandedge features. The unilluminated region, Figure 4-6(b), is much thinner than the illuminated region, and there is no bandedge feature in the PL. This indicates that the growth conditions were not optimum for eliminating Zn vacancies and min-

ZnSe Growth #	*50*	*28*	*51*
Growth Time (Hr)	4	4	4
T_{sub} (^oC)	250	355	460
Cracker T_{Se} (^oC)	800	800	800
Cracker T_{Zn} (^oC)	50	50	50
DESe flow rate (sccm)	0.5	0.5	0.5
DEZn flow rate (sccm)	2.5	2.5	2.5
Laser λ Å	4579	4579	4579
Unilluminated thickness Å	1100	1000	700
Illuminated thickness Å	9200	3000	1100

Table 4.3: Growth conditions for the comparison of the PL for the ZnSe grown using DEZn and DESe with different substrate temperatures.

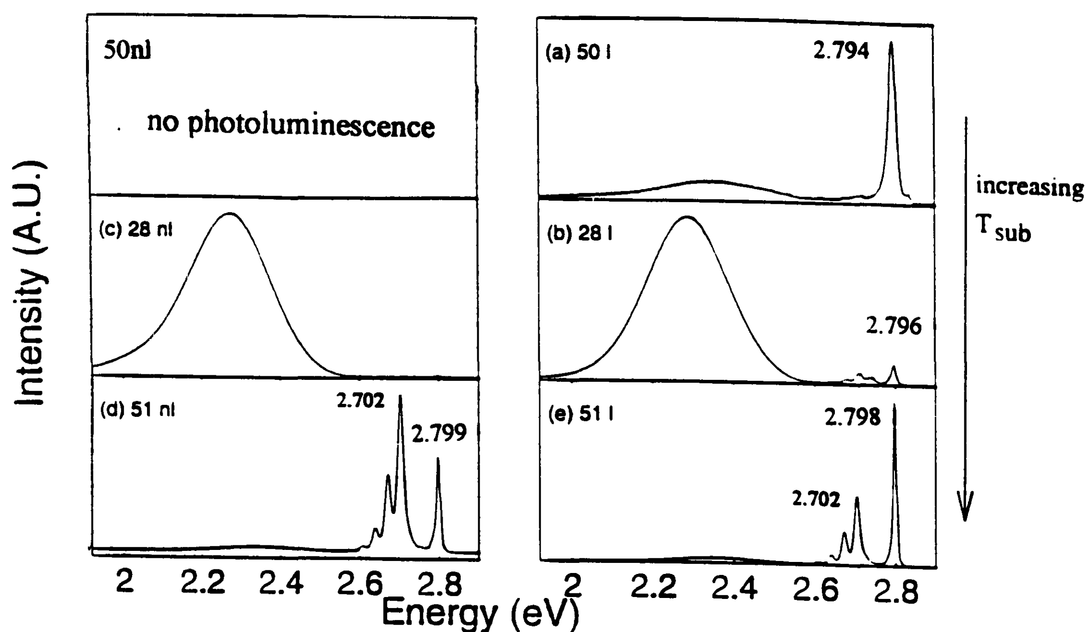

Figure 4-6: PL of ZnSe grown using DEZn and DESe with different substrate temperatures (T_{sub}). (a) 250°C, (b) and (c) 355°C, (d) and (e) 460°C. All of the nl samples are pseudomorphic.

imizing defects due to nonstoichiometry. The presence of bandedge features for the illuminated regions indicates that laser illumination created photogenerated carriers which react with the Zn complexes at the surface to break apart any bonds between Zn and ethyl radicals, which reduces the number of Zn vacancies, and hence, reduces the intensity of the defect band PL feature relative to the bandedge features [8]. To the left of the donor-bound exciton feature at 2.796 eV of Figure 4-6(c), there is donor acceptor pair (DAP) transition at 2.737 eV accompanied by phonon replicas.

The highest growth temperature has the best PL in relation to eliminating the defect band. Figures 4-6 (d) and (e) show the PL for growth # 51 without and with laser illumination, respectively. The intensity of the self-activated emission (2.38 eV) is relatively small compared to the bound exciton features. In addition, the laser illuminated portion of growth # 51 has a more intense donor-bound exciton feature with respect to the DAP feature than the unilluminated region of the sample. This reduction could possibly be due to a decrease in the concentration of acceptors or an increase in the concentration of donors in the laser-assisted areas of the film. The origin of the DAP feature in growth # 51 is different from the DAP feature previously seen.

The improvement in the ratio between the intensity of the bandedge features to the defect band as the growth temperature increases is explained by the effect of substrate temperature on the DEZn molecule. At the higher growth temperatures, the DEZn molecule is more efficiently pyrolyzed at the sample surface. Therefore, more Zn is incorporated and the concentration of Zn vacancies is reduced. Laser illumination during growth improves the optical quality by breaking up the ethyl radicals, leaving less DEZn at the sample surface hence, the level of Zn vacancies is reduced.

Variations in Zn flux

A comparison of the PL from ZnSe films grown with different Zn fluxes is made in Figure 4-7. The growth parameters (Table 4.4) have been set such that a moderate substrate temperature, ~355°C, is maintained when the zinc flux was varied from 2 to 0.5 sccm; the Se flux was held constant at 0.5 sccm. The resulting PL for each case shows a progression in the relative intensities between the bandedge features and the defect band. The comparison is more vivid for the laser-assisted areas of the samples. As the growth conditions become increasingly Zn-rich, the defect band decreases in magnitude, suggesting a decrease in the Zn vacancies which are a source of point defects.

The DAP features in the unilluminated regions (Figures 4-7 (a) and (c)) differ from the DAP features in the illuminated regions (Figure 4-7 (d) and (f)) of the ZnSe films. For the unilluminated regions, the DAP feature and the donor-bound exciton feature form one unresolved feature. The PL for the illuminated regions show separate DAP and donor-bound exciton features. The origin of the DAP feature in both regions is speculated to be due to a deep donor (carbon) recombining with an acceptor. It is speculated that the concentration of the zinc vacancies is higher for the unilluminated regions of the samples than for the illuminated regions.

Summary

In summary, the three comparisons have shown various trends in the PL of ZnSe that was grown using DEZn and DESe sources. First, when the energy of the laser used in the laser-assisted growth of ZnSe is greater than the defect state energies, the PL for the regions with laser assistance has a higher crystalline quality over the regions without laser assistance. The improvement in crystal quality is manifested by a reduction in the relative intensities of the defect band to the bandedge features. Second, increasing the sample temperature during growth reduces the magnitude of the defect band with respect to the bandedge features. This is accompanied by a slight improvement in the resolution of the bound exciton and the DAP features. Finally, increasing the Zn flow rate improves the film quality. This is seen in both

ZnSe Growth #	*54*	*55*	*53*
Growth Time (Hr)	4	4	4
T_{sub} (^{o}C)	360	355	355
Cracker T_{Se} (^{o}C)	800	800	800
Cracker T_{Zn} (^{o}C)	50	50	50
DESe flow rate (sccm)	0.5	0.5	0.5
DEZn flow rate (sccm)	2	1	0.5
Laser λ Å	4579	4579	5145
Unilluminated thickness Å	1000	1100	1100
Illuminated thickness Å	4400	4500	3000

Table 4.4: Growth conditions for the comparison of the PL for different Zn fluxes.

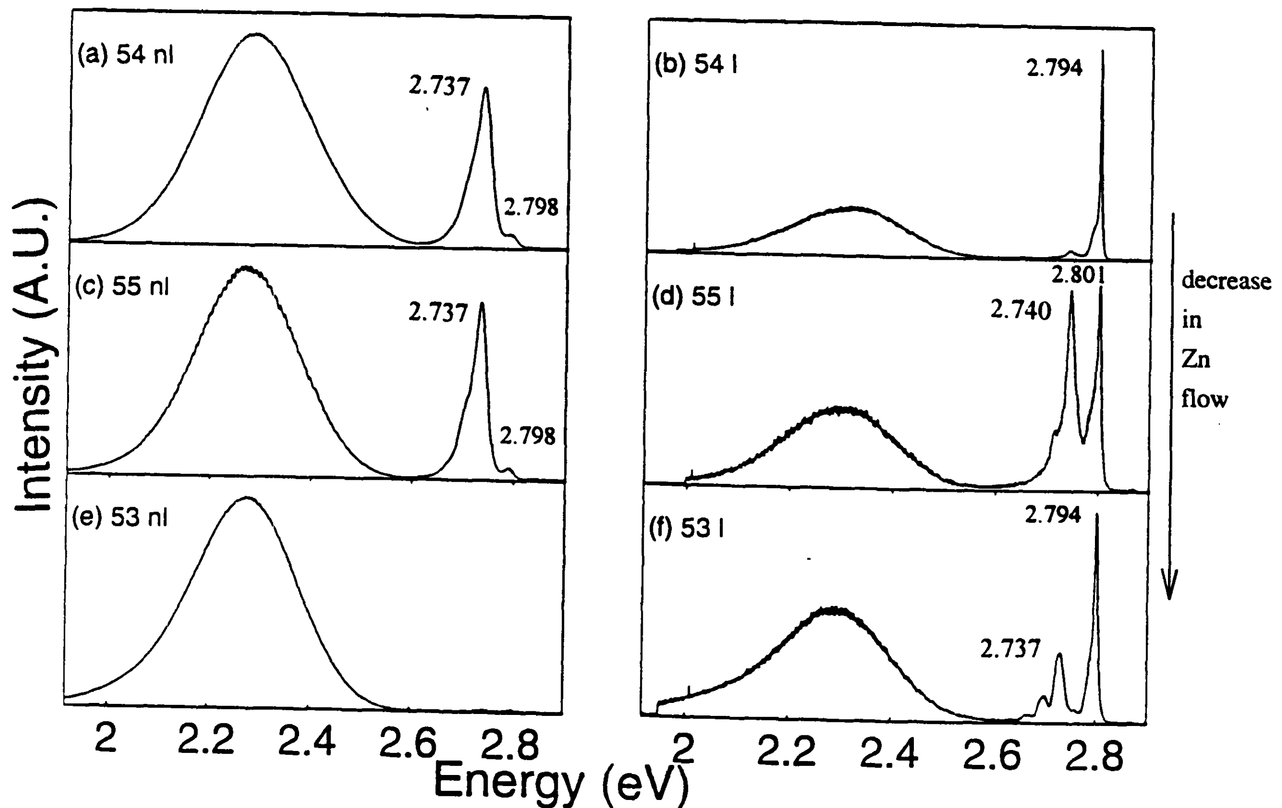

Figure 4-7: PL of ZnSe grown using DEZn and DESe with different Zn fluxes. (a) and (b) 2 sccm, (c) and (d) 1 sccm, (e) and (f) 0.5 sccm. The nl samples are pseudomorphic to the GaAs.

the unilluminated and the illuminated regions of each sample where the ratio of the intensities of the bandedge features to the defect band feature decreases as the Zn flow rate increases. These three comparisons correlate the PL with the difficulty in incorporating the Zn atom during MOMBE growth with DEZn and DESe sources. The use of the ethyl-based sources causes a surface site blockage due to a strongly bound chemisorbed species at the surface prohibiting incorporation of the metal atoms. The use of photo-assistance with energies above the bandgap result in increasing the Zn incorporation via a photo-catalytic effect involving free carriers and the adsorbed DEZn molecule.

4.1.2 ZnSe Grown with One Diethyl-Based Source and One Elemental Source

Only one ZnSe film that was grown using this combination of sources; DEZn and elemental Se (Table 4.5) had a detectable level of PL. While no comparisons can be made within this subset of MOMBE growth, the PL of this film, Figure 4-8, is useful for comparisons across the entire range of MOMBE experiments. At a relatively low growth temperature of 280 °C, a thin ZnSe film was grown (both regions are much thinner than the critical thickness). The resulting PL shows that both the illuminated and the unilluminated regions of the sample is defect-dominated. However, the film is very thin, and from a measurement standpoint, the fact that there was a detectable level of luminescence from the sample suggests good crystal quality. Since the PL measurement has probed to the ZnSe/GaAs interface, the appearance of bandedge features in the illuminated region of the sample indicates that the laser is effective in reducing vacancies even during the initial stages of the nucleation. Also, the presence of the defect band for an elemental Se source means that the defect band is not solely a function of the DESe source used in the previous analysis.

ZnSe Growth #	*65*
Growth Time (Hr)	1
T_{sub} (^oC)	280
Effusion Cell T_{Se} (^oC)	250
Cracker T_{Zn} (^oC)	50
Laser λ Å	4579
Unilluminated thickness Å	200
Illuminated thickness Å	500

Table 4.5: Growth conditions for ZnSe grown with DEZn and solid Se.

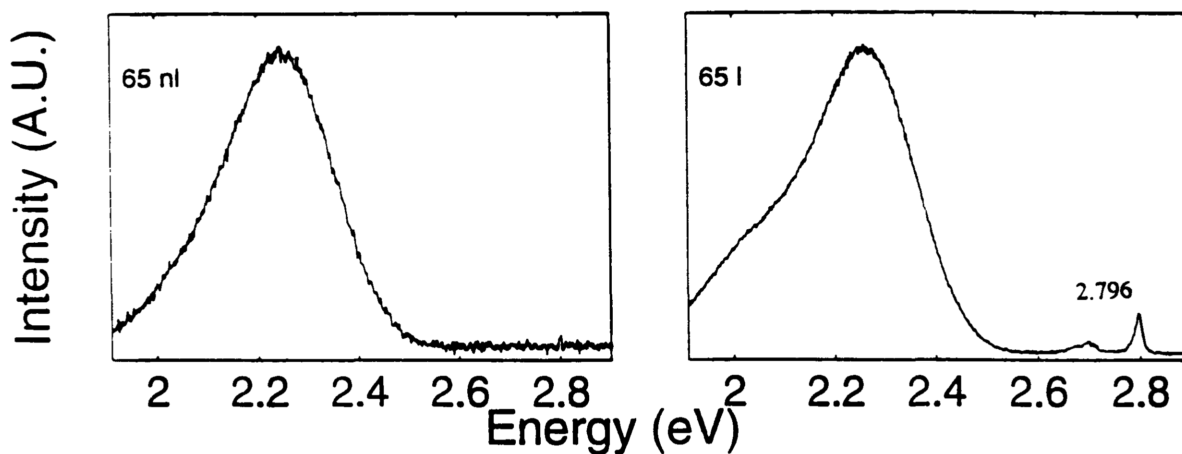

Figure 4-8: PL of ZnSe grown using DEZn and elemental Se.

ZnSe Grown with Elemental Zn and DESe Sources

Three of the films that were grown using elemental Zn and DESe sources (Table 4.6) were grown where both the substrate temperature and the Zn cell temperature were varied. The PL for these samples, Figure 4-9, is shown for only the unilluminated regions since in growth # 63, ZnSe did not nucleate in the illuminated region, and in growth # 66, the laser illumination suppressed the ZnSe growth rate which resulted in a film which was too thin to optically characterize. For the combination of elemental Zn and DESe sources, the laser has an effect on the Se atom. Excess Se is desorbed in the laser-assisted regions of the sample and the Zn is not affected [7]. Each of the resulting films are very thin. Growths # 66 and 63 were grown with both moderate substrate and Zn effusion cell temperatures. The resulting PL spectra are defect-dominated, indicating that the ethyl radicals from the DESe are blocking the incorporation of Zn into the lattice leading to point defects. For a very low growth temperature (235°C), and a moderate Zn effusion cell temperature, the PL indicates that the ZnSe has high crystalline quality (Figure 4-9 (a)). The primary PL feature for this sample is a donor-bound exciton transition, however, an intense free exciton feature appears as well. Since the temperature of the Zn effusion cell dictates the magnitude of the Zn deposition rate, the moderate Zn cell temperature could be high enough to reduce the presence of Zn vacancies during the ZnSe deposition.

The laser illuminated regions of the ZnSe films grown with elemental Zn and DESe experienced a suppressed growth rate, indicating that the laser is desorbing the Se atoms from the sample surface. As the Se flux is increased, or the growth temperature is decreased, laser-assisted growth has less of an effect on the resultant ZnSe; this is speculated to be a Se desorption phenomenon [30].

ZnSe Growth #	*66*	*63*	*69*
Growth Time (Hr)	1	1	1
T_{sub} (^oC)	300	280	235
Cracker T_{Se} (^oC)	800	800	800
Effusion Cell T_{Zn} (^oC)	440	335	360
Unilluminated thickness Å	300	300	675

Table 4.6: Growth conditions for the comparison of the PL for the ZnSe grown with solid Zn and DESe sources for different growth temperatures and Zn fluxes.

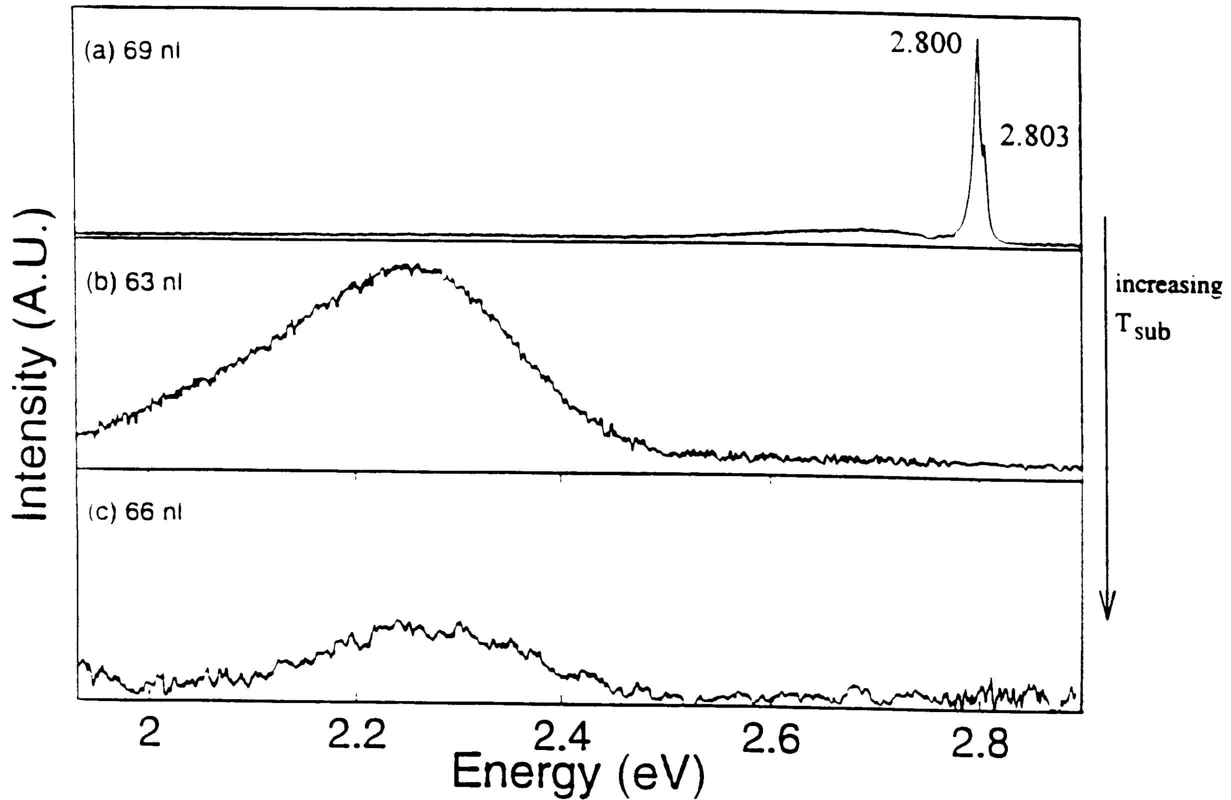

Figure 4-9: PL of ZnSe grown using Zn and DESe with different substrate temperatures and Zn fluxes. (a) T_{sub} = 235°C, T_{Zn}=360°C, (b) T_{sub} = 280°C, T_{Zn} = 335°C, (c) T_{sub} = 300° C, T_{Zn} = 440° C.

4.1.3 ZnSe Grown with One Dimethyl-based Source

ZnSe films that were grown using DMZn and solid Se as sources for different growth temperatures (Table 4.7) have markedly different optical properties in comparison to films grown using ethyl-based sources. The PL of the methyl-based samples are shown in Figure 4-10. Once again, the primary feature in the PL is the defect band. However, at higher substrate temperatures, the shape of the defect band changes from a single peak centered at around 2.3 eV to two peaks centered at 2.0 eV and 2.4 eV. As the growth temperature decreases, the illuminated regions show an increase in the ratio of the intensities of the bandedge features to the defect band. In the unilluminated cases, at lower T_{sub}, the bandedge features barely exist; while at the higher T_{sub}, they are greater than or comparable to the intensity of the defect band. The bandedge features are primarily the emission from a donor-bound exciton and a DAP transition. The shape of the band edge features implies that there are two different DAP features; one corresponding to a deep donor level, and the other to a shallow donor level (Figures 4-10 (a) and (c)). The illuminated regions of the films are either thinner than or roughly equal to the same thickness as the unilluminated regions, most of which are below the critical thickness. The suppression of the ZnSe growth rate using laser illumination suggests that the laser does not have the same effect on DMZn that it does on DEZn. In the PL of the methyl-based ZnSe films, the laser affects the optical properties, because the bandedge features are enhanced with respect to the defect band at lower substrate temperature (Figures 4-10 (e) and (f)). The effects of the laser-assisted growth are also found in the samples grown with a higher T_{sub} (Figure 4-10 (a) and (b)). In this situation, the bandedge feature is reduced with respect to the defect band for the PL of the unilluminated sample with increasing substrate temperature. In either case, increasing the sample temperature during growth is reducing the amount of Zn at the surface, and increasing the number of vacancies as a result.

ZnSe Growth #	*97*	*93*	*96*
Growth Time (Hr)	1	1	1
T_{sub} (^oC)	280	310	330
Effusion cell T_{Se} (^oC)	234	222	234
Cracker T_{Zn} (^oC)	1050	1050	1050
DMZn flow rate (sccm)	1	1	1
Laser λ Å	4579	4579	4579
Unilluminated thickness Å	1450	1250	1450
Illuminated thickness Å	1850	1000	1000

Table 4.7: Growth conditions for the comparison of the PL for the ZnSe grown using DMZn and solid Se sources for different growth temperatures.

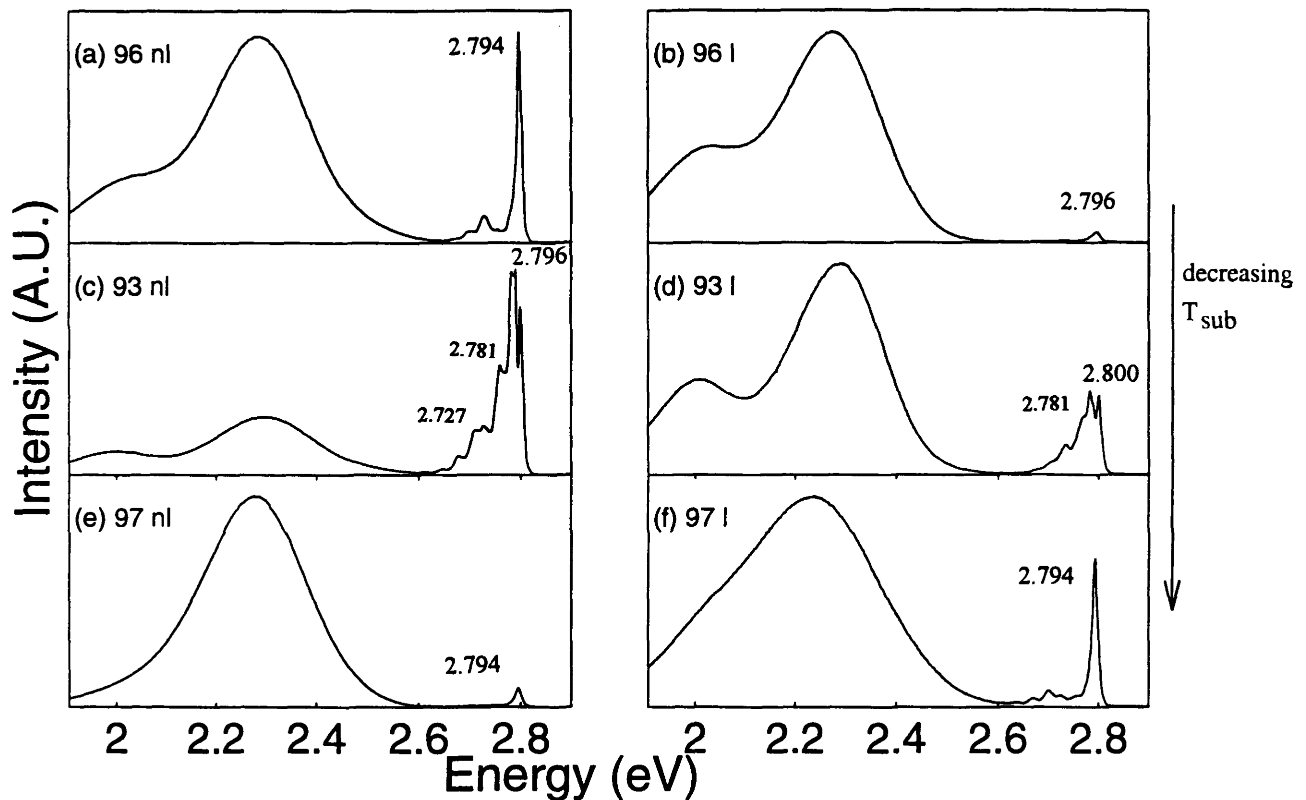

Figure 4-10: PL of ZnSe grown using DMZn and elemental Se with different substrate temperatures, (T_{sub}). (a) and (b) 330°C, (c) and (d) 310°C, (e) and (f) 280°C.

ZnSe Grown using DMZn and Elemental Se with Different Zn Flow Rates

Another comparison can be made by considering the ZnSe growth rate as the DMZn flow rate was varied. Three films were grown under similar conditions for one hour, with large variations in the resulting film thickness (Table 4.8). At the highest DMZn flow rate, both the illuminated and the unilluminated regions are the thickest of the three growths; well above the critical thickness, suggesting that the Zn arrival rate limits the growth rate. In the other two samples, the films are below or approximately equal to the critical thickness (1500 Å). The laser has the effect of suppressing the growth at the lower two DMZn flow rates, while enhancing the growth at the higher flow rate. Figure 4-11 shows the PL for three samples with Zn flow rates of 1, 1.5, and 2 sccm. There are three trends evident in the PL. First, in the laser-assisted areas of the samples, the ratios of the intensities of the defect band to the bandedge structure are increasing with decreasing DMZn flow rates. Secondly, for an increase in DMZn flow rate, the relative intensities between the donor bound exciton and the deep level DAP transition features increases regardless of whether laser illumination occurred on the sample during growth or not. However, the PL of the film grown using the lowest DMZn flow rate, Figures 4-11 (a) and (b), has a stronger shallow DAP transition feature than donor-bound exciton feature. Finally, in the comparison between the laser illuminated and unilluminated case, the presence of a shallow donor in a DAP transition occurs for higher substrate temperatures in the illuminated laser case (Figures 4-11 (a), (b), and (c)). The appearance of the shallow donor-acceptor pair is speculated to be a function of the level of carbon incorporation in the film. As the carbon level decreases, the shallow donor level has a higher probability of radiative recombination with an acceptor level. Higher carbon concentrations effectively saturate the level, and force any radiative recombinations from the shallow donor level to a deep donor level. In growth # 93, a shift in the DAP transition energy is seen. Two DAP features exist, accompanied by phonon replicas. The smaller of the two DAP features in intensity corresponds to the same transition as shown for the growth #'s 98 and 99. The other DAP transition has

ZnSe Growth #	*93*	*98*	*99*
Growth Time (Hr)	1	1	1
T_{sub} (^{o}C)	310	310	310
Effusion cell T_{Se} (^{o}C)	222	234	234
Cracker T_{Zn} (^{o}C)	1050	1050	1050
DMZn flow rate (sccm)	1	1.5	2
Laser λ Å	4579	4579	4579
Unilluminated thickness Å	1250	2300	2800
Illuminated thickness Å	1000	1900	3800

Table 4.8: Growth conditions for the comparison of the PL for the ZnSe grown using DMZn and solid Se sources for different Zn flow rates.

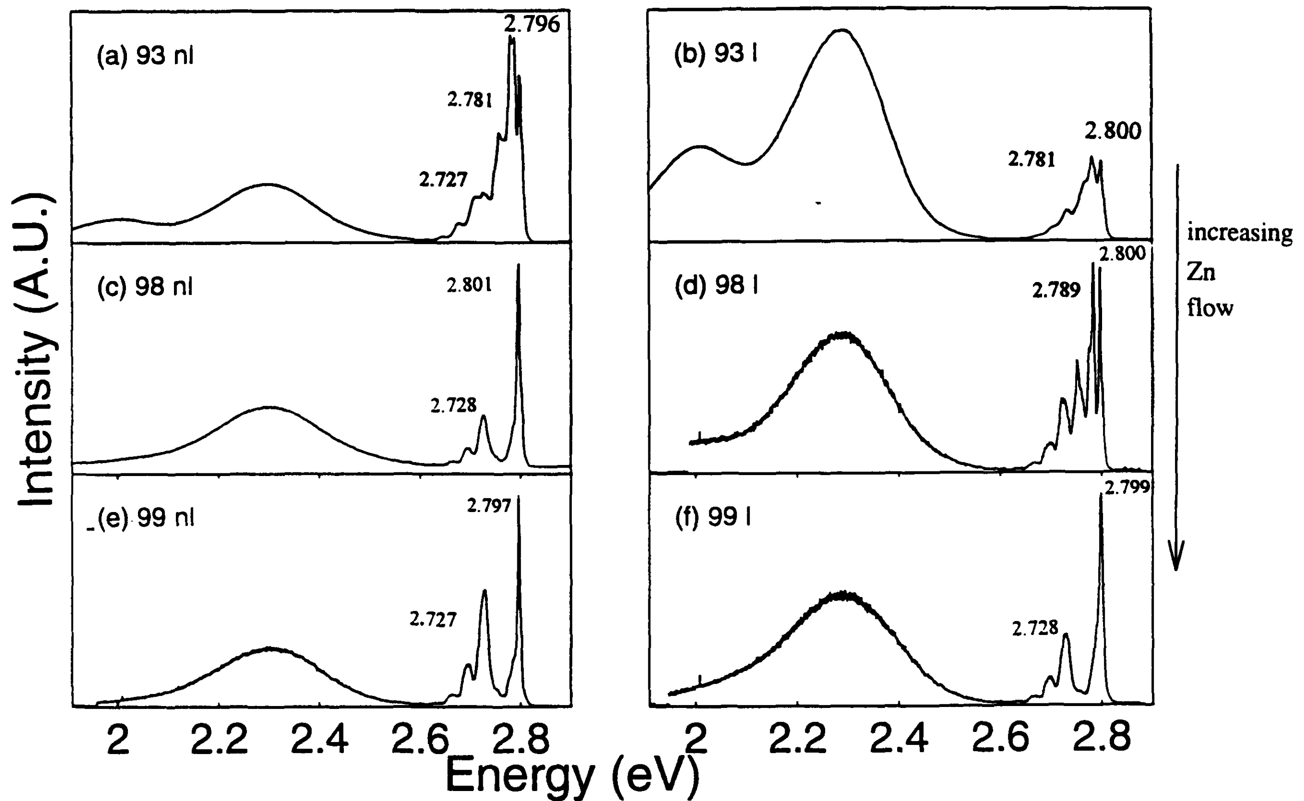

Figure 4-11: PL of ZnSe grown using DMZn and elemental Se with different Zn fluxes (a) and (b) 1 sccm, (c) and (d) 1.5 sccm, (e) and (f) 2 sccm.

a higher energy, and hence corresponds to a change from a deep donor state to a shallow donor. The combination of the improved ratios of the donor-bound exciton to the defect band intensities, the improved ratios of the donor-bound exciton to the deep DAP transition, and the presence of the shallow DAP transition with increasing Zn fluxes suggests that the higher DMZn flow rates are effective in improving the optical quality of the ZnSe film.

ZnSe grown using DMZn and DESe.

The growth of ZnSe using DMZn and DESe was performed once. The growth conditions are shown in Table 4.9. For a standard growth time of 1 hour, and a moderate substrate temperature of 310°C, the resulting ZnSe film is very thin in both the laser illuminated and the non-illuminated regions. However, a detectable level of PL from a region of the sample which did not have laser-illumination during growth was collected (Figure 4-12). The PL is defect-dominated, as shown by the defect band at $\sim$ 2.3 eV. The primary band-edge feature corresponds to a donor-bound exciton structure at 2.799 eV. The illuminated region emitted no detectable level of luminescence. The fact that the thicknesses of the two regions on the sample are comparable suggests that the laser had little effect on the growth rate.

ZnSe grown with DMZn and H_2Se sources

The last case of growth which employs one metal-organic source is ZnSe grown with DMZn and H_2Se, and falls under the category of CBE. Four films were grown under the same conditions except for variations in the substrate temperature (Table 4.10). The films are all much thicker than the critical thickness. The resulting PL (Figure 4-13) is defect dominated. The only film which has any recognizable bandedge features is shown in Figure 4-13 (d). When the measurement was taken, the other three films luminesced a bright orange, which indicates an abundance of states throughout the band-gap. Since the orange luminescence has never been seen in the previous MOMBE samples, the combination of the sources implemented and the very low growth temperatures in growth #'s 114-116 could have resulted in a high concentration of point defects throughout the film.

ZnSe Growth #	*94*
Growth Time (Hr)	1
T_{sub} (^oC)	310
Cracker T_{Se} (^oC)	800
Cracker T_{Zn} (^oC)	1050
DMZN flow rate (sccm)	1
DESe flow rate (sccm)	0.5
Laser λ Å	4579
Unilluminated thickness Å	250
Illuminated thickness Å	300

Table 4.9: Growth conditions for ZnSe grown using DMZn and DESe.

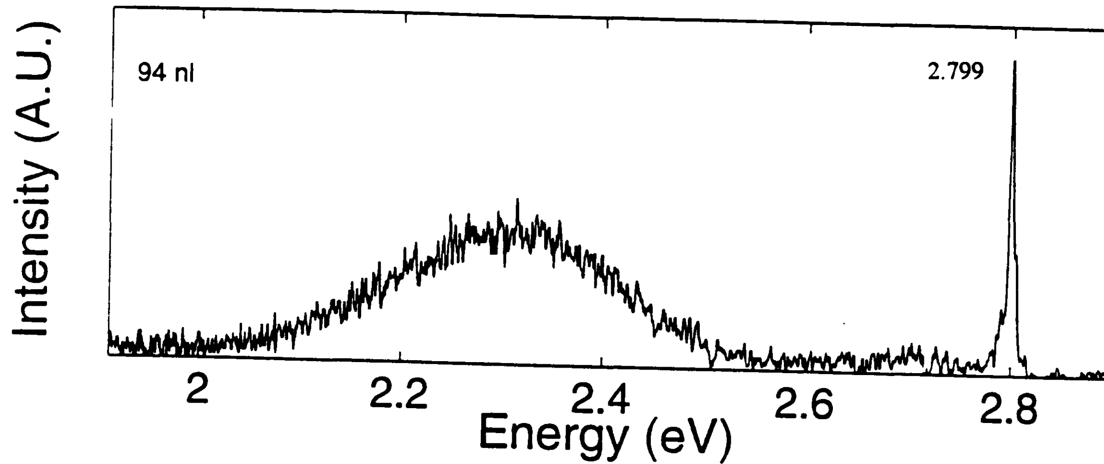

Figure 4-12: PL of ZnSe grown using DMZn and DESe.

ZnSe Growth #	*113*	*114*	*115*	*116*
Growth Time (Hr)	3	3	3	3
T_{sub} (^oC)	310	250	220	200
Cracker T_{Se} (^oC)	1200	1200	1200	1200
Cracker T_{Zn} (^oC)	1050	1050	1050	1050
DMZN flow rate (sccm)	2	2	2	2
H_2Se flow rate (sccm)	1	1	1	1
Unilluminated thickness μm	0.52	0.82	0.7	0.65

Table 4.10: Growth conditions for the comparison of the PL of ZnSe grown using DMZn and H_2Se for different growth temperatures.

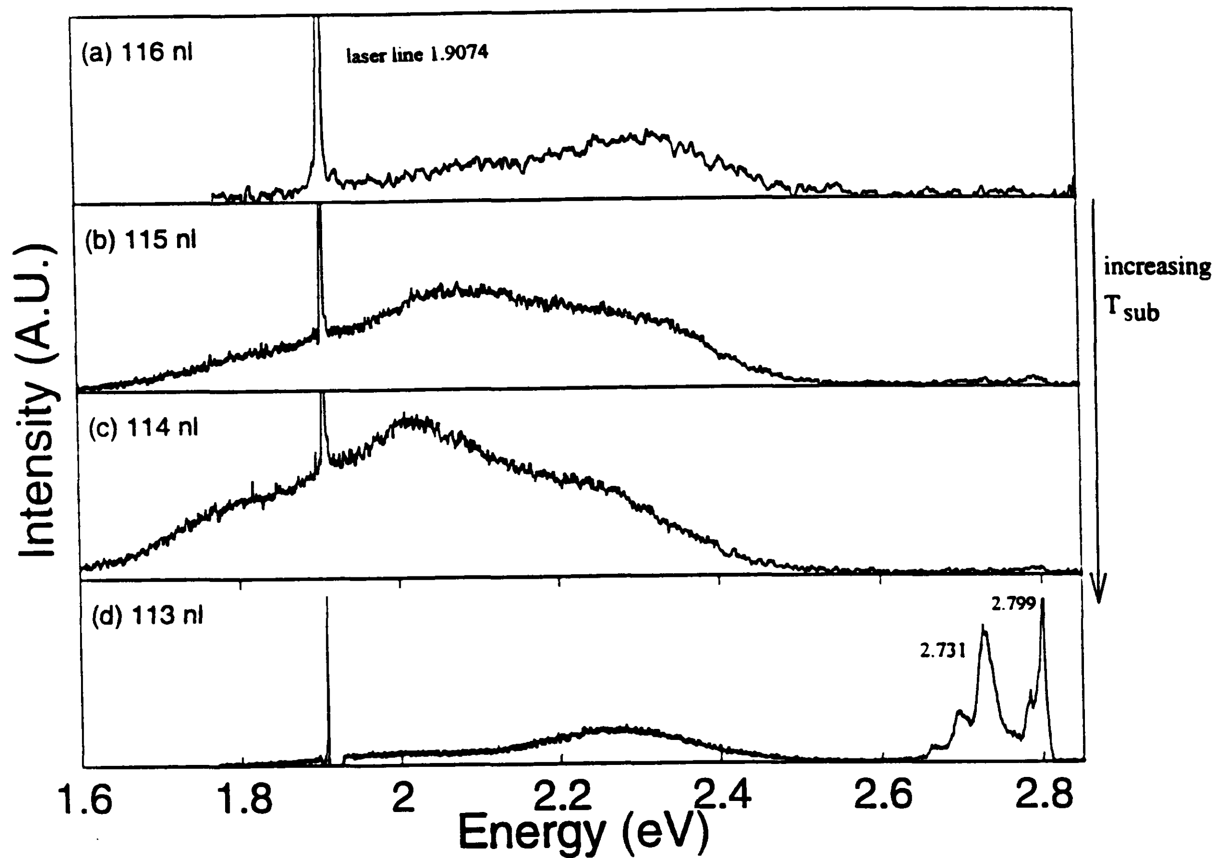

Figure 4-13: PL of ZnSe grown using DMZn and H_2Se for different growth temperatures, (T_{sub}). (a) 200°C, (b) 220°C, (c) 250°C, (d) 310°C.

4.2 ZnSe Grown by MBE

Most ZnSe-based optical devices are grown by MBE [2, 3, 4]. For the sake of growth rate comparisons, MBE was used during the growth of several films. However, the growth conditions were widely varied except for the case of three films, where the substrate temperature was the sole variable (Table 4.11). No nucleation was achieved for the film attempted with a T_{sub} of 380 °C (growth # 82), since the Zn and Se desorbed from the sample surface during growth. Only one of the films (growth # 68) had a detectable PL signal, as shown in Figure 4-14. The PL in Figure 4-14 shows a high quality ZnSe film, with a small defect band and a dominant bandedge feature. The primary features at the bandedge are due to a donor-bound exciton at 2.800 eV and a deep donor-acceptor-pair at 2.737 eV. The ZnSe grown by MBE can yield PL dominated by a free exciton feature as in the case of the ZnSe used in light emitting diode structures [2]. However, the PL of growth # 68 does not exhibit this ideal. The presence of a defect band indicates that the film was grown with nonstoichiometric growth conditions. The presence of a donor-bound exciton indicates a high impurity concentration.

4.3 ZnSe Grown by GSMBE

The optical properties of the ZnSe grown by GSMBE has also been investigated. In GSMBE, elemental Zn and gaseous H_2Se are used as source materials. In addition, the growth rate is limited only by mass transport. An example of the surface uniformity of a GSMBE-grown ZnSe film is shown in Figure 4-15, where PL measurements are made at several points on a sample. The FWHM and the transition energy of the donor-bound exciton feature remains constant across the sample.

The GSMBE ZnSe epilayers were grown with the optical and electrical properties in mind; hence, there are more complete sets of data for comparison. Because the optical properties are under consideration, the films are thicker (usually $> 1\mu$ m). Therefore, compressive strain is no longer the primary consideration in the PL fea-

ZnSe Growth #	*81*	*68*	*82*
Growth Time (Hr)	1	1	1
T_{sub} ($^{\circ}C$)	220	300	380
Effusion Cell T_{Se} ($^{\circ}C$)	219	220	219
Effusion Cell T_{Zn} ($^{\circ}C$)	338	338	338
Unilluminated thickness Å	1800	1175	0
Illuminated thickness Å	1800	1025	0

Table 4.11: Growth conditions for the comparison of the PL for the ZnSe grown using elemental Zn and elemental Se.

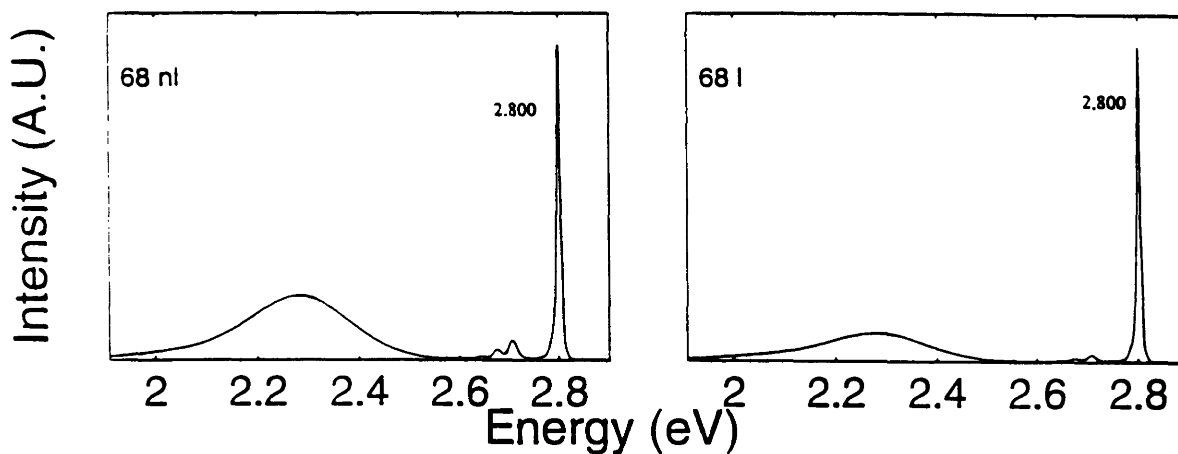

Figure 4-14: PL of ZnSe grown using elemental Zn and elemental Se.

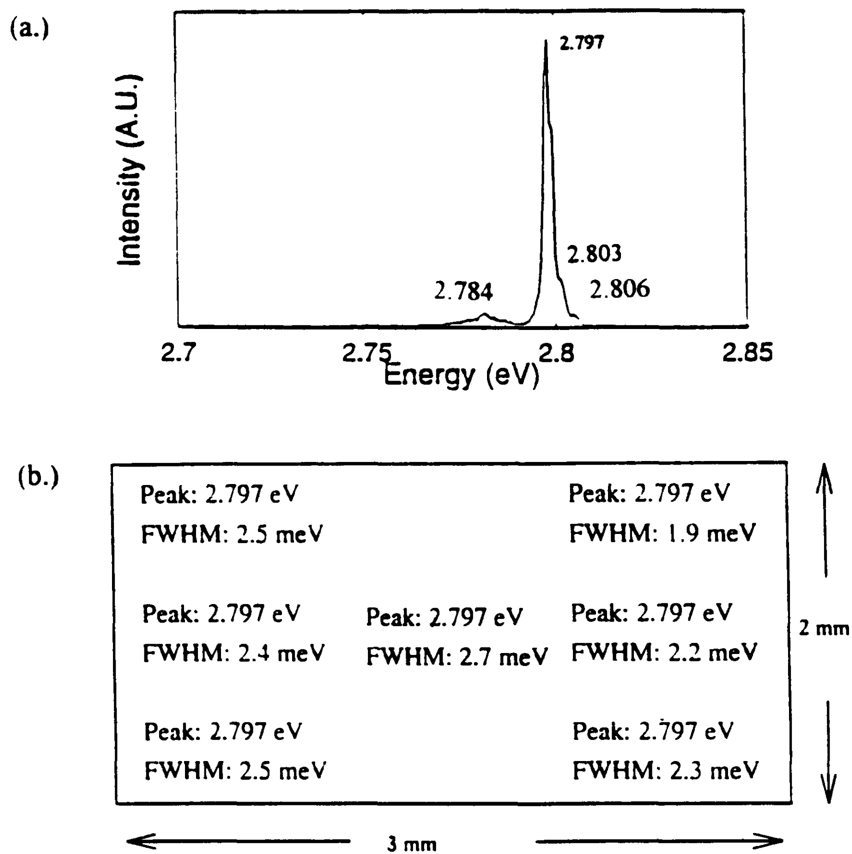

Figure 4-15: (a) PL of a GSMBE sample. (b) The peak energies and FWHM's of the PL at the respective locations on the sample.

ture energies. Instead, the film experiences tensile strain when being cooled to the measurement temperature.

Along with the surface uniformity, the dependence of the integrated intensity of the bandedge features of the PL for a GSMBE-grown ZnSe film on the PL measurement temperature was determined. For a range of energies which includes all of the bandedge PL features, the PL of a ZnSe sample was taken at several measurement temperatures. The combination of the changes in the FWHM and peak intensities can be defined by the integrated intensity. Figure 4-16(a) shows the integrated intensity for a GSMBE-grown ZnSe film as a function of the measurement temperature. The integrated intensity decreases, falling by 80% from 10 K to 77 K, as the PL measurement temperature increases. At room temperature, the integrated intensity is 5% of the 10 K value. The corresponding 10 K PL of the ZnSe is shown in Figure 4-16(b). Although the PL for this sample is dominated by bandedge features, the primary feature is the donor-bound exciton structure at 2.798 eV. The free exciton (FE) structure appears as a shoulder to the right of the donor-bound exciton feature. As the PL measurement temperature increases, the exciton gains enough energy to 'unbind' from the impurity becoming a free exciton. As a result, the donor-bound exciton feature decreases with increasing PL measurement temperature. Depending on the quality of the ZnSe, the free exciton can either radiatively or nonradiatively recombine. For a film with a lot of trap states, the free exciton is more likely to recombine nonradiatively, hence further decreasing the PL intensity of the bandedge features. Therefore, the integrated intensity as a function of PL measurement temperature effectively measures the quality of the ZnSe. For a high quality ZnSe film, the integrated intensity will decrease more slowly with PL measurement temperature. In comparison to the MOMBE samples, where the PL tended to be defect-dominated and the measure of crystal quality was a function of the defect band, the PL of the GSMBE-grown ZnSe films does not exhibit a defect band structure. Thus, the integrated intensity is a useful measure of the relative quality of the GSMBE-grown ZnSe films.

Several comparisons are made of the PL from the GSMBE-grown ZnSe films. First,

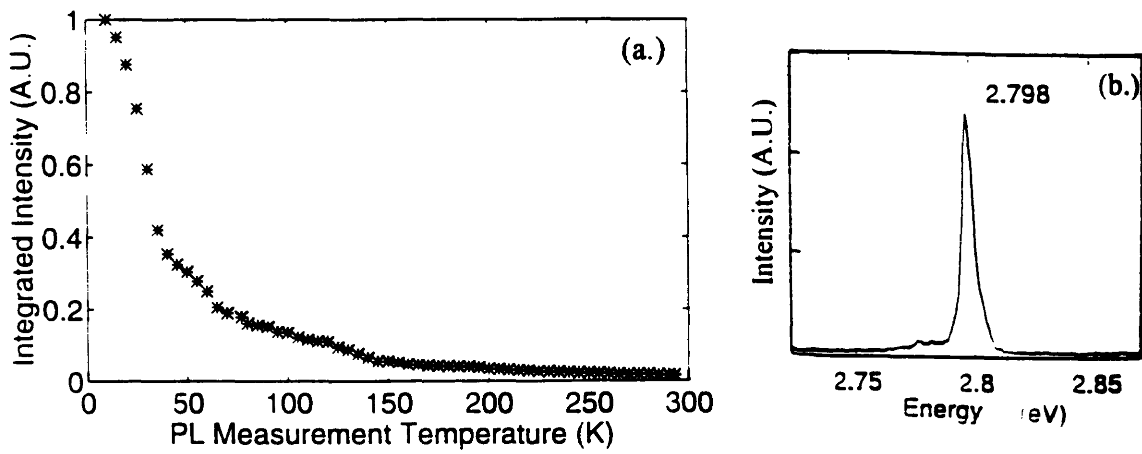

Figure 4-16: (a) Integrated intensity of a GSMBE-grown ZnSe film as a function of PL measurement temperature. (b) PL of GSMBE-grown ZnSe film used for the integrated intensity measurement.

the PL for epilayers grown with different substrate temperatures is considered. This comparison is further supported by taking PL measurements at a higher temperature (77 K) to investigate the defect-related features, such as DAP transitions. Also, the PL for ZnSe films grown with different H_2Se cracker temperatures and with different Zn fluxes is compared.

ZnSe with different substrate temperatures

Five GSMBE growths with similar growth conditions, except T_{sub}, were completed (Table 4.12). However, the parameters have been varied to achieve slightly Zn- or Se-rich stoichiometry. Growth #'s 120, 121, and 122 are considered Se-rich based upon the corresponding RHEED reconstructions during the growths; whereas growths 124 and 125 are considered Zn-rich. The corresponding PL, Figure 4-17, shows little or no defect band, and the primary feature at 2.798 eV is a donor bound exciton arising from chlorine impurities [24]. The films are under tensile strain due to the low PL measurement temperature, with the corresponding shift in the feature energies by +2 meV.

As the growth temperature increases, a more prominent free exciton (FE) feature appears at 2.803 eV in the PL spectra. The FE transition corresponds to a light hole state in the valence band since the film is under tensile strain. The presence of a FE feature in the PL indicates a higher optical quality ZnSe film, since the concentration of impurities and vacancies in the lattice has been reduced to the point that a pure band-edge transition is detectable. The FE feature appears for lower T_{sub}'s in the Zn-rich case (270°C) than for the Se-rich case (300°C).

For the PL taken at 77 K, the primary features are the same as the lower temperature measurement (Figure 4-17 (b)). However, the energies shift slightly to lower energies due to the different measurement temperature since the bandgap energy of a material is temperature dependent. For the lowest growth temperature, the defect band structure appears. In this case, the ratio of the intensities of the donor-bound exciton feature to the defect band is $\sim$100. Therefore, even at higher PL measurement temperatures the ZnSe film exhibits good optical characteristics.

ZnSe Growth #	*122*	*124*	*125*	*120*	*121*
Growth Time (Hr)	4	4	4	4	4
T_{sub} (^oC)	250	274	290	315	330
Cracker T_{Se} (^oC)	1000	1000	1000	1000	1000
Effusion Cell T_{Zn} (^oC)	305	304	304	305	305
Se flow rate (sccm)	2.5	1.8	1.8	2.5	2.5
Zn flux (Å/sec)	0.73	0.71	0.75	0.68	0.77
Thickness μm	2.2	1.17	1.15	1.55	1.55

Table 4.12: Growth conditions for the comparison of the PL for the ZnSe grown using solid Zn and H_2Se with different substrate temperatures.

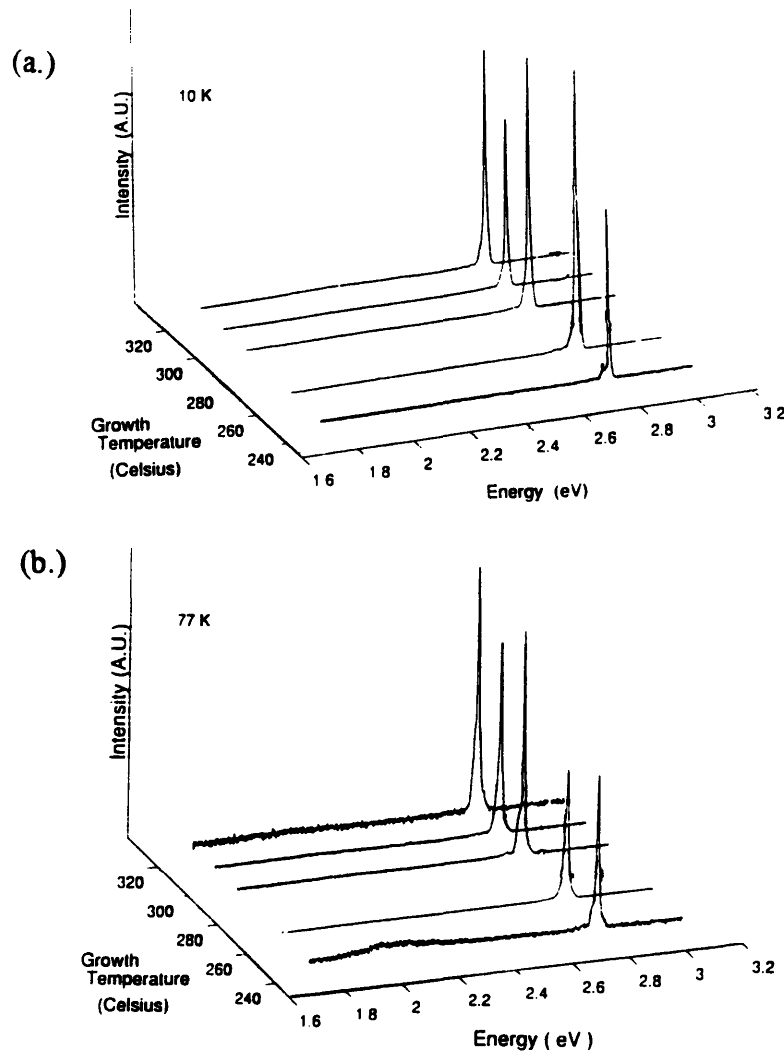

Figure 4-17: PL of ZnSe grown using solid Zn and and H_2Se with different substrate temperatures. PL measurements made (a) at 10 K, (b) at 77 K.

ZnSe with different H_2Se cracking cell temperatures

Three ZnSe samples were grown with variations in the H_2Se cracking cell temperature while maintaining a constant Zn flux. The other growth parameters are similar (Table 4.13), with a slight variation in the Zn cell temperature. The thickness of the resulting films increase with increasing cracking cell temperatures. The PL spectra of these films are shown in Figure 4-18, where, once again, the primary feature corresponds to the donor-bound exciton transition at 2.798 eV. While decreasing the cracking cell temperature significantly decreases the growth rate due to less cracked H_2Se at the surface, the resultant PL indicates higher crystalline quality with the presence of the FE transition at 2.802 eV. Since the Zn flux remained constant, the II-VI ratio at the surface increases with decreasing cracking cell temperatures. Also, a donor-bound exciton feature at 2.797 eV exists in the PL for growth # 155. The shift in the donor-bound exciton feature is a function of the thickness of the ZnSe films as can be seen in the increase in peak energies. Since the thickness of growth # 155 is 1800 Å, the ZnSe is potentially under a slightly compressive strain, which is manifested by a increase in the donor-bound exciton energy.

As the cracking cell temperature decreases, the corresponding PL features become sharper, with narrower FWHM values. In growth #'s 159 and 158, the donor-bound exciton features are convolved with the LO phonon replicas. The features in growth # 155 are more resolved, with the FE peak at 2.804 eV appearing as both a narrow feature, but $\sim$ 30% as intense as the donor-bound exciton feature. The improvement in the ZnSe optical properties with lower H_2Se cracking cell temperatures is a function of the availability of Zn at the ZnSe surface during growth. Lowering the cracking cell temperature effectively reduces the Se concentration at the ZnSe surface, increasing the Zn-to-Se ratio at the ZnSe surface. Zn-rich growth conditions improve the optical properties of the resulting ZnSe.

ZnSe Growth #	*158*	*159*	*155*
Growth Time (Hr)	3	3	3
T_{sub} ($^{\circ}C$)	270	270	270
Cracker T_{Se} ($^{\circ}C$)	800	700	600
Effusion Cell T_{Zn} ($^{\circ}C$)	309	307	309
Se flow rate (sccm)	1.7	1.7	1.7
Zn flux (Å/sec)	0.98	1.01	1.03
Unilluminated thickness μm	1.30	0.72	0.18

Table 4.13: Growth conditions for the comparison of the PL for the ZnSe grown using solid Zn and H_2Se with different cracker cell temperatures.

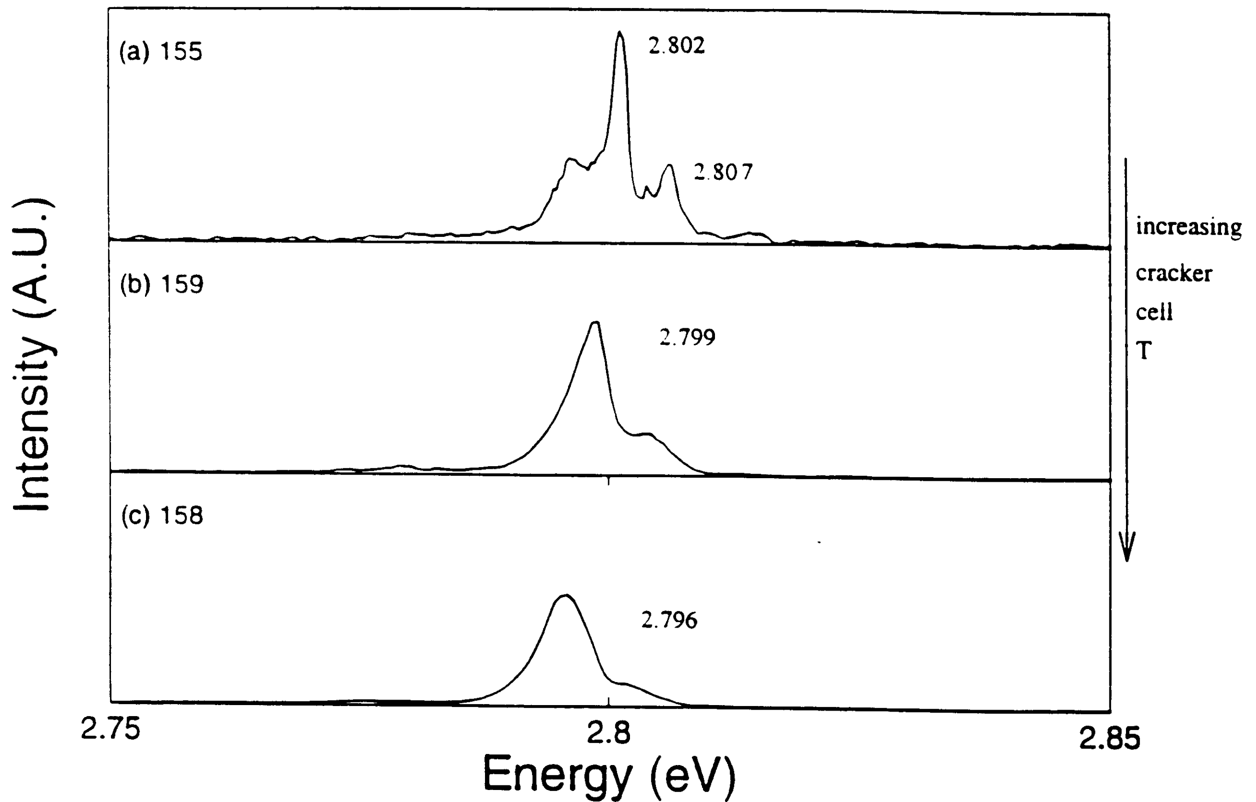

Figure 4-18: PL of ZnSe grown using solid Zn and and H_2Se with different cracking cell temperatures.(a) 600°C (b) 700°C, (c) 800°C.

ZnSe with different Zn fluxes

The growth parameters for three ZnSe samples which were grown by GSMBE with variations in Zn flux are shown in Table 4.14. The corresponding PL (Figure 4-19) shows three spectra which are similarly dominated by bandedge features. However, as the Zn flux is increased, the different features at the bandedge become more resolved. The primary feature is a donor-bound exciton feature at 2.798 eV. Another feature which appears as a shoulder on the donor-bound exciton feature for the PL of growth # 118 is speculated to be a shallow donor-bound exciton feature. To the far right, a FE structure appears at 2.803 eV. In all three cases, the donor-bound exciton structure is present, along with the FE structure. The appearance of the shallow donor-bound exciton structure indicates a decrease in the impurity concentration.

Although the PL spectra are similar for variations in Zn flux, there is a slight improvement in the crystalline quality for higher Zn fluxes. As the Zn flux is increased, the growth rate also increases, indicating that the growth is Zn-limited.

Summary

The photoluminescence of ZnSe grown by GSMBE improves for more Zn-rich growth conditions. For higher substrate temperatures or Zn oven temperatures, the FE transition increases in intensity, which is an indication of good optical properties. Lowering the H_2Se cracker cell temperature has the same effect. Because of the presence of the FE structure, for the first time in the ZnSe PL, the donor-bound exciton structure could be associated with MOMBE sources. As the number of GSMBE samples have been grown, the donor-bound exciton feature at 2.798 eV has decreased in relative intensity.

4.4 Doping of ZnSe

ZnSe was doped both p-type and n-type using GSMBE. For p-type doping, the dopant is nitrogen; for n-type doping, the dopant is chlorine. Photoluminescence is useful for qualitative analysis of the relative doping concentrations for variations in the growth

ZnSe Growth #	*117*	*120*	*118*
Growth Time (Hr)	4	1	1
T_{sub} (^oC)	300	315	300
Cracker T_{Se} (^oC)	1000	1000	1000
Effusion Cell T_{Zn} (^oC)	297	305	303
Zn flux Å/sec	0.55	0.68	0.73
Unilluminated thickness μm	1.0	1.6	1.55

Table 4.14: Growth conditions for the comparison of the PL for the ZnSe grown using solid Zn and H_2Se with different Zn fluxes.

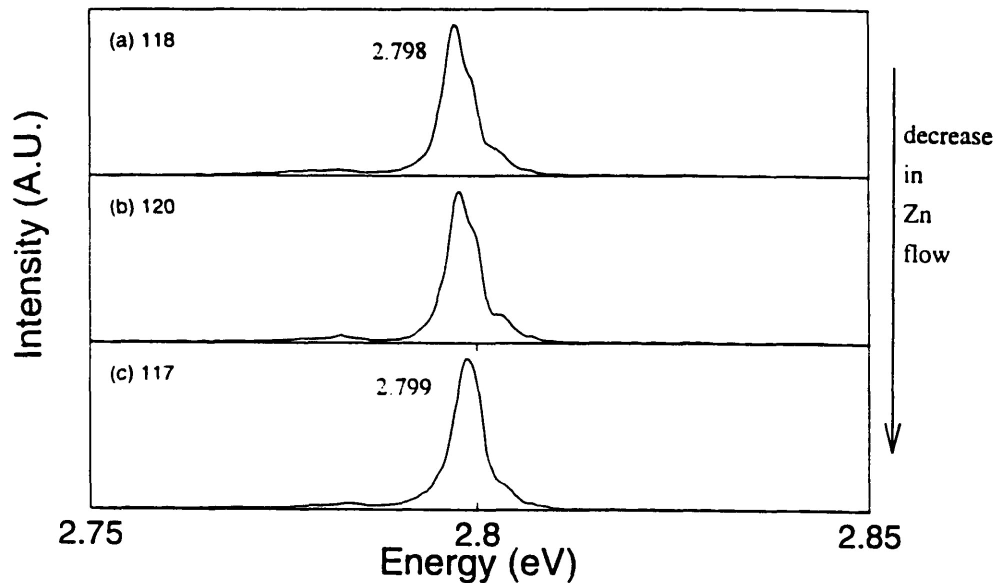

Figure 4-19: PL of ZnSe grown using solid Zn and and H_2Se with different Zn fluxes. (a) 0.73 Å/sec (b) 0.68 Å/sec (a) 0.55 Å/sec.

parameters. The p-type doping of ZnSe was achieved using a nitrogen plasma source, while the n-type doping was achieved with a $ZnCl_2$ solid source. The PL for both cases of ZnSe doping is presented and discussed in the next two subsections. The comparisons for both p-type and n-type doping are for variations in the respective dopant's parameter space.

4.4.1 ZnSe:N

The combination of nitrogen doping and GSMBE is a new contribution to the study of ZnSe growth [9]. With the experiments to date, two comparisons can be made for variations in the plasma source's RF power and for variations in N_2 background pressure. When a nitrogen plasma source is used to generate the nitrogen for p-type doping, an RF power supply creates atomic nitrogen species that incorporate into the ZnSe lattice. Hence, variations in the RF power alter the amount of nitrogen available for doping. At a substrate temperature of 250°C, three ZnSe films were grown with different RF powers, Table 4.15. All of the films are much thicker than the critical thickness. Figure 4-20 shows the PL for the three samples. The primary feature for each case is near 2.7 eV, and corresponds to a donor-acceptor pair transition. As the RF power increases, the feature broadens and merges with the LO phonon replicas. The broadening of the DAP transition has been observed for increasing doping concentrations [31, 32]. Hence, for increasing RF power, the doping concentration of the ZnSe film increases. This is confirmed by secondary ion mass spectroscopy measurements where the nitrogen concentration increases from 4.5 x 10^{17} to 2 x 10^{18}, and finally to 5 x 10^{18} as the RF power increases from 100 W to 200 W and finally to 300 W, respectively.

For the p-type doping, there is a dependence on the primary PL feature energy, corresponding to either a deep or shallow donor level, for different nitrogen concentrations (Figure 4-22 (a)). As the RF power increases, the primary PL feature shifts to a lower energy, as the DAP is made of a deep donor level and the nitrogen acceptor state (Figure 4-22 (b)) [31]. The shift to a deep donor level is also seen in the shape of the DAP transition feature on the PL. As the deep donor level becomes the

ZnSe Growth #	*142*	*145*	*146*
Growth Time (Hr)	5	5	5
T_{sub} (^oC)	250	250	250
Cracker T_{Se} (^oC)	1000	1000	1000
Effusion Cell T_{Zn} (^oC)	312	311	311
Se flow rate (sccm)	1.2	1.2	1.2
Zn flux (Å/sec)	0.96	0.97	0.97
N_2 Background Pressure (10^{-5} Torr)	2.0	2.0	2.0
RF Power (W)	100	200	300
Unilluminated thickness μm	1.85	1.95	2.05

Table 4.15: Growth conditions for the comparison of the PL for the p-type ZnSe grown by GSMBE with different RF powers.

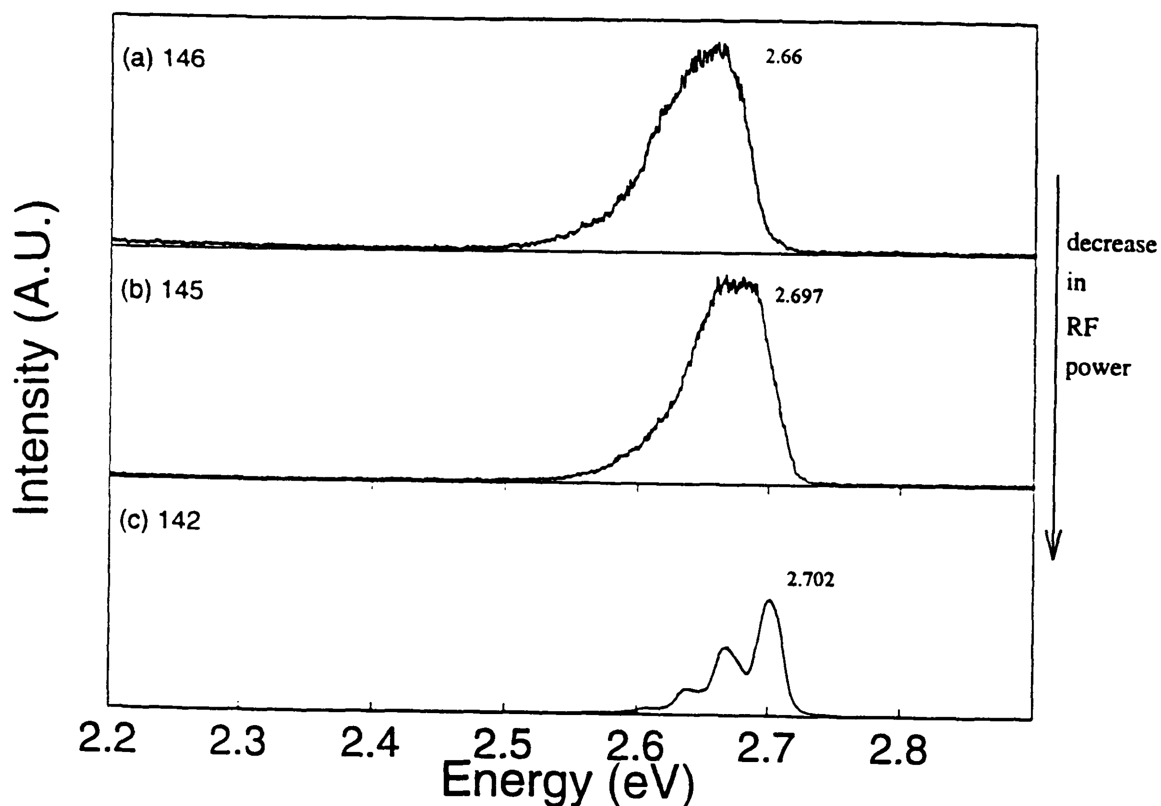

Figure 4-20: PL of ZnSe:N grown by GSMBE with different RF powers. (a) 300 W, (b) 200 W, (c) 100 W.

prominent donor state for the donor-acceptor pair, the LO phonon replicas corresponding to the deep level DAP increase in intensity and effectively broaden the PL feature.

ZnSe:N with different N_2 background pressures

Another comparison can be made for variations in the background pressure of N_2 during the growth of p-type ZnSe. Three films were grown under similar conditions with different background pressures, Table 4.16. The films are thick, close to 2 μm. The resultant PL is shown in Figure 4-21. The primary feature at $\sim$ 2.7 eV corresponds to a deep DAP transition. For each of the films, though, a broadening in the DAP at a slightly lower energy indicates the presence of a shallow level DAP feature [31]. As the background pressure of N_2 is increased, the PL feature broadens. The broadening of the bandedge feature indicates an increase in nitrogen doping levels as the shallow nitrogen level has a high enough concentration of electrons to participate in a detectable level of radiative recombinations.

ZnSe Growth #	*131*	*129*	*127*
Growth Time (Hr)	5	5	5
T_{sub} (^oC)	270	270	280
Cracker T_{Se} (^oC)	100	1000	1000
Effusion Cell T_{Zn} (^oC)	304	304	304
Se flow rate (sccm)	1.5	1.5	1.5
Zn flux (Å/sec)	0.72	0.7	0.71
N_2 Background Pressure (10^{-5} Torr)	2.1	0.97	0.45
RF Power (W)	100	100	100
Unilluminated thickness μm	1.90	2.0	1.95

Table 4.16: Growth conditions for the comparison of the PL for the ZnSe:N grown by GSMBE with different N_2 background pressures.

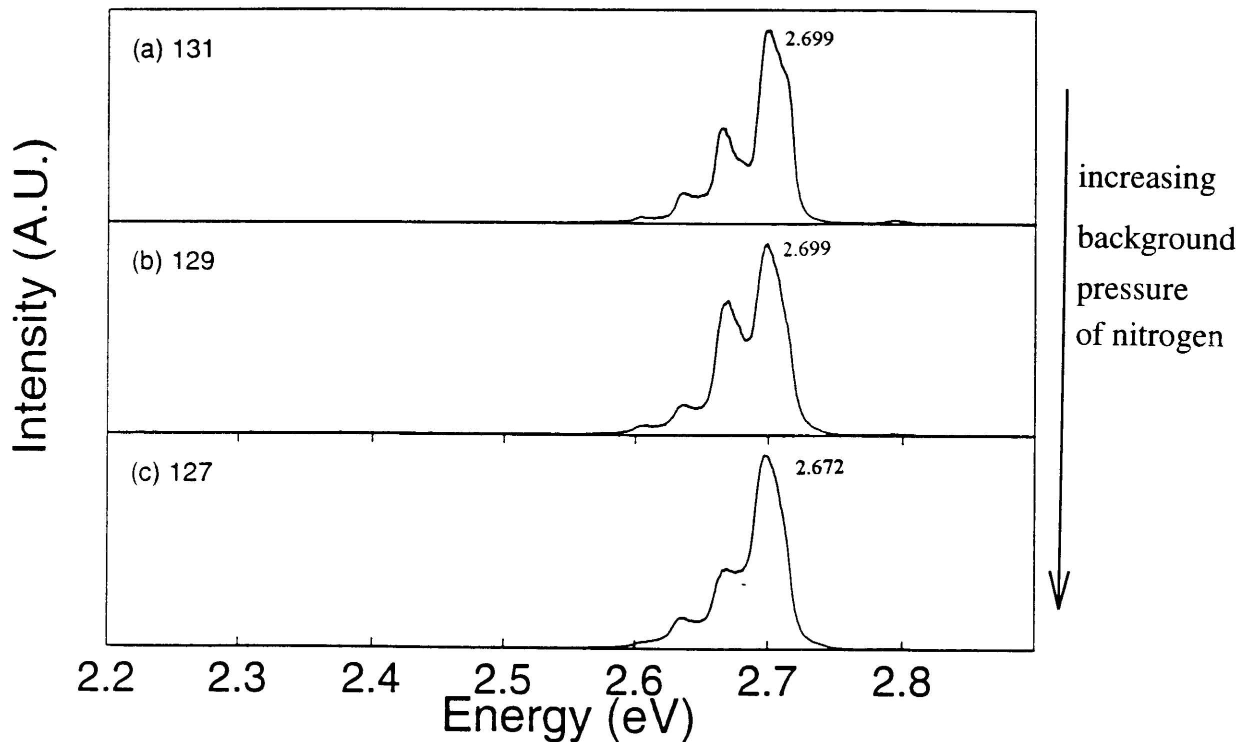

Figure 4-21: PL of ZnSe:N grown by GSMBE with different N_2 background pressures. (a)$2.1x10^{-5}$ Torr, (b) $9.7x10^{-6}$ Torr (c)$4.5x10^{-6}$ Torr.

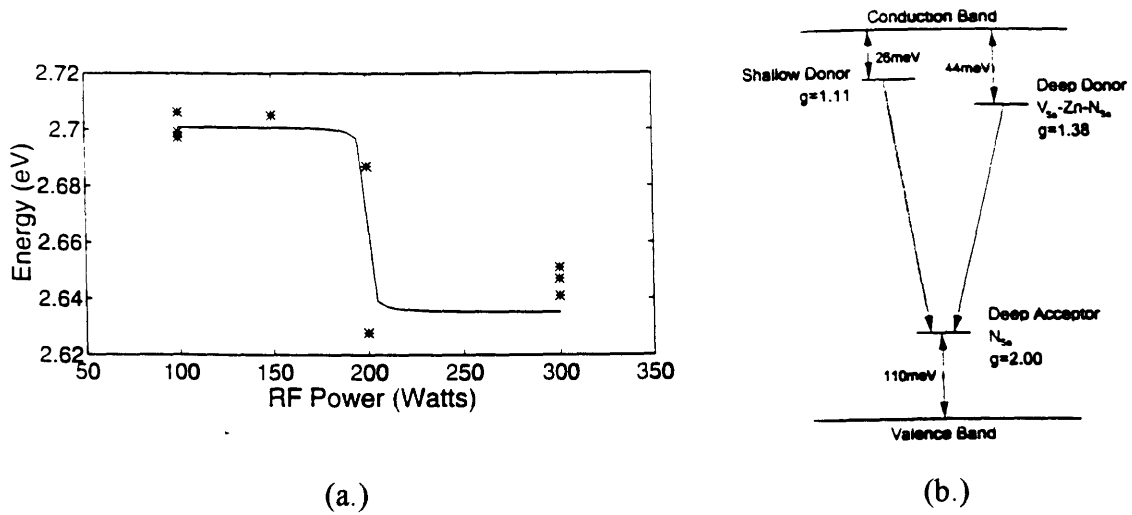

(a.) (b.)

Figure 4-22: (a) Plot of the energy of the donor-acceptor-pair transition in the PL of nitrogen doped ZnSe. (b) Flat band depiction of deep and shallow nitrogen donor levels in ZnSe [30].

4.4.2 ZnSe:Cl

Three n-type ZnSe samples were grown by GSMBE with variations in the $ZnCl_2$ cell temperature. The growth conditions are shown in Table 4.17. All of the films are above the critical thickness, $\sim 2\ \mu$m. As a result, tensile strain due to the different thermal expansion coefficients of ZnSe and GaAs result in a shift in the feature energies by + 2 meV [15]. Furthermore, increasing the $ZnCl_2$ cell temperature increases the doping level. This can be seen in the corresponding PL in Figure 4-23 where the primary feature, the donor-bound exciton at 2.795 eV, corresponding to a deep donor impurity, grows in intensity for increasing T_{ZnCl_2} (Figure 4-24). At a slightly higher energy, a shoulder corresponding to the shallow donor level is present that is $\sim$ 50% as intense as the bound exciton feature corresponding to the deep donor level.

ZnSe Growth #	*164*	*162*	*163*
Growth Time (Hr)	3	3	3
T_{sub} ($^\circ C$)	295	290	290
Cracker T_{Se} ($^\circ C$)	1000	1000	1000
Effusion Cell T_{Zn} ($^\circ C$)	322	322	322
ZnCl Cell T_{ZnCl} ($^\circ C$)	150	170	190
Unilluminated thickness μm	2.40	2.25	2.13

Table 4.17: Growth conditions for the comparison of the PL for the ZnSe:Cl grown by GSMBE with different $ZnCl_2$ cell temperatures.

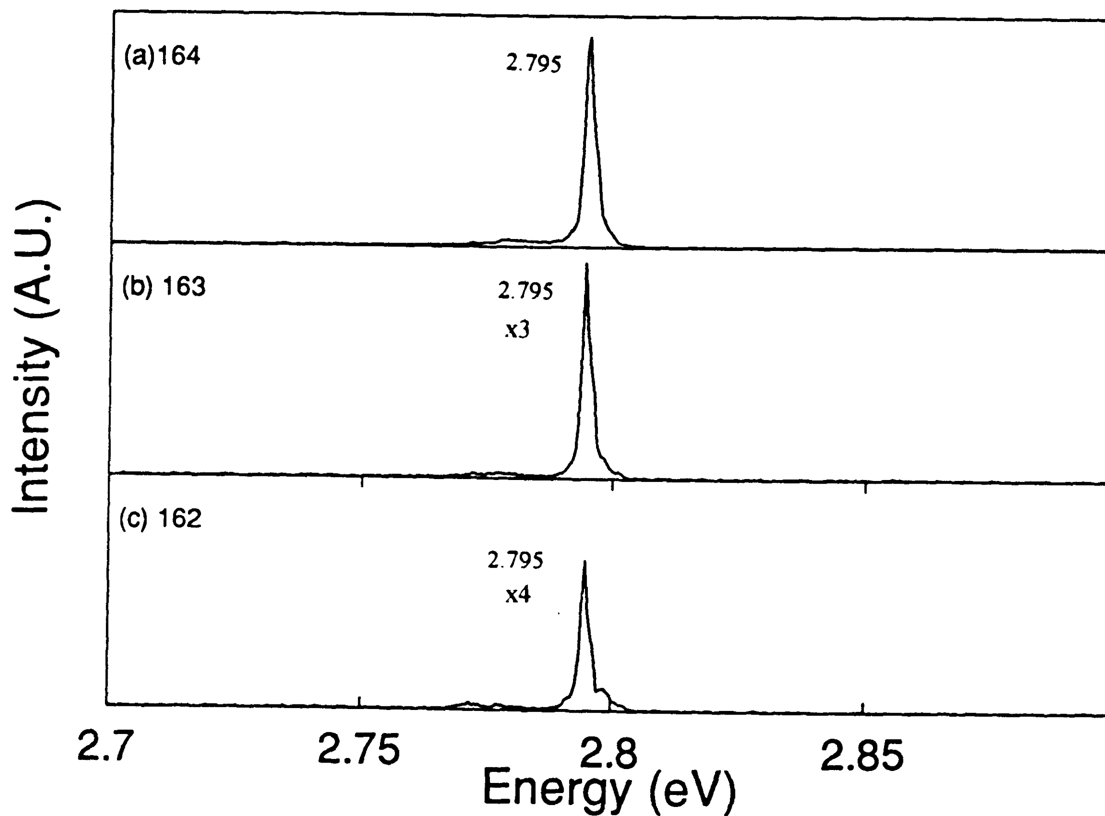

Figure 4-23: PL of ZnSe:Cl grown by GSMBE with different $ZnCl_2$ cell temperatures (a) 150°C, (b) 170°C, (c) 190°C.

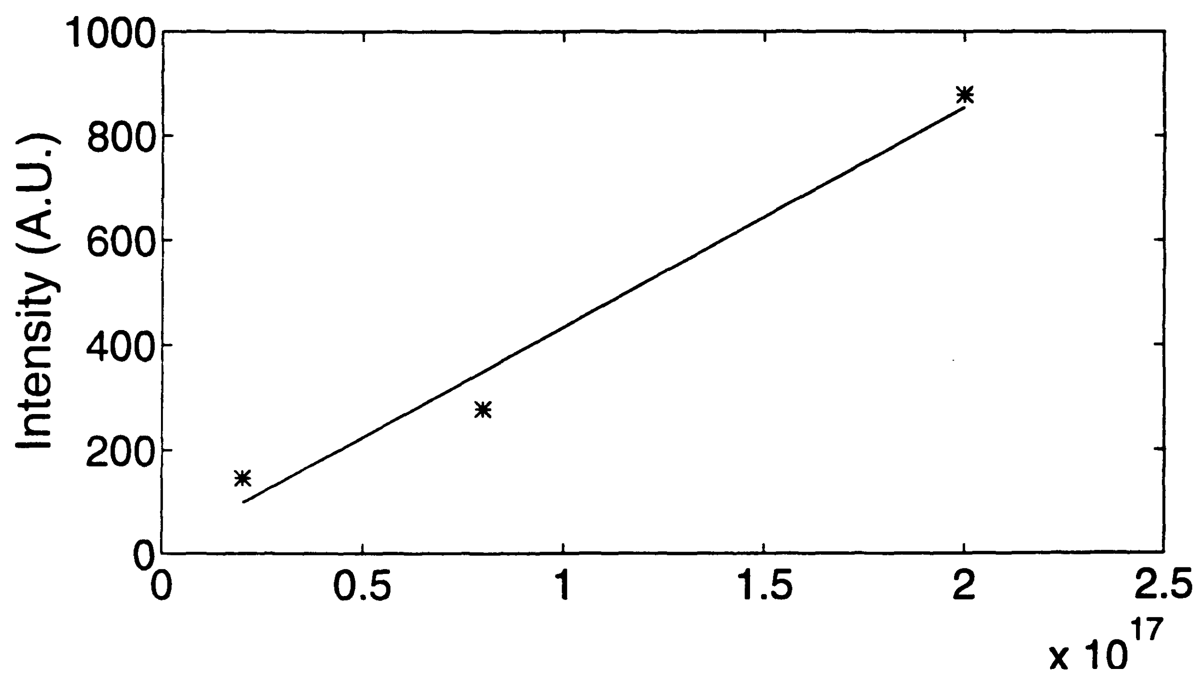

Figure 4-24: Plot of the intensity of the donor-bound exciton feature in the PL of chlorine-doped ZnSe.

Chapter 5

Summary

In an attempt to optimize the ZnSe film quality and the growth rate, several growth parameters have been varied. Also, different types of sources have been used for the constituent species: metal-organic gases, solid elemental, and gaseous hydrides. The introduction of either a p-type dopant, nitrogen, or a n-type dopant, chlorine, in the ZnSe has also affected the optical properties. Along with these dopant studies the effects due to the substrate temperature, the behaviour of the constituent species, and laser-assisted growth on the optical properties of ZnSe have been examined.

As the sources used to epitaxially grow the ZnSe have been varied, the primary effect on the optical characteristics, as seen in the PL, has been the presence of impurities from the sources. For the ZnSe films grown by MOMBE, a carbon impurity inherent to the ethyl- and methyl-based sources is speculated to be the impurity in the PL in both the donor-bound exciton features and the donor-acceptor-pair features. When DMZn is used in the growth, both shallow and deep donor levels from the carbon are detected from the DAP features in the PL. For the MBE-grown ZnSe, a carbon donor-bound exciton feature dominates the PL. However, since the MBE films were grown in the same chamber as the MOMBE films, the presence of carbon in the MBE-grown ZnSe films is speculated to be a residual "memory effect" from the metal-organic sources. For the GSMBE-grown ZnSe, chlorine is the prominent impurity (confirmed by secondary ion mass spectrosopy measurements). The identification of the chlorine donor bound exciton transition in the PL is further supported by the

energy of the primary feature in the ZnSe:Cl which corresponds to a donor-bound exciton. Finally, the presence of nitrogen in ZnSe:N is exhibited by the presence of a DAP feature accompanied by LO phonon replicas.

The PL of ZnSe yields information about the film's stoichiometry. The majority of the MOMBE-grown ZnSe films are defect dominated, as determined by a large defect band feature in the corresponding PL. Zn vacancies resulting from nonstoichiometric growth conditions allow for an almost continuous band of states in the energy gap. Hence, a wide ($\sim$ 1 eV) range of luminescence is detected in the PL. For MBE-grown ZnSe, the defect band is also present. However, in the GSMBE-grown ZnSe films, the absence of a defect band feature in the PL indicates that stoichiometric growth conditions have been achieved. For 77 K PL measurements of the GSMBE-grown ZnSe films, the defect band remains more than an order of magnitude smaller than the bandedge features.

The presence of the ZnSe PL features are dependent on the impurities present in the sources employed in the growth. The energies of the PL features are temperature dependent due both the lattice mismatch and the different thermal expansion coefficients in the ZnSe/GaAs heterostructure. However, the growth temperature and thickness of the ZnSe films often vary together since the films were grown for a uniform duration at a given growth temperature and the growth rate was temperature dependent. A trend in the energy of the donor-bound exciton feature as a function of ZnSe thickness cannot be determined because there is a great deal of scatter in the data points due to variations in the growth temperature. The MOMBE-grown ZnSe films have thicknesses which are below and close to the critical thickness of 1500 Å. As a result, the energy of the donor-bound exciton feature is strongly dependent on the film thickness. Also, the substrate temperature changes the energies of the bandedge features. For the GSMBE films, the thicknesses far exceed the critical thickness, and only a small shift in the donor-bound exciton energy ($<$ 1 meV) results with respect to the film thickness.

The PL for the ZnSe films has also shown an improvement in the optical properties for an increase in the Zn flux at the surface, independent of the sources used. As

the Zn flux increases for the MOMBE-grown films, the ratio of the intensities of the donor-bound exciton feature to the defect band increases. Furthermore, as the growth temperature decreases for the MOMBE grown ZnSe films, where an elemental Zn source was used, the same intensity ratio increases, indicating an improvement in the ZnSe optical properties. For the GSMBE ZnSe films, the free exciton feature in the PL increases in intensity relative to the intensity of the donor-bound exciton feature as the Zn flux increases.

Within the subset of MOMBE-grown ZnSe, the laser-assisted regions have been analyzed. There are three effects of the laser on the ZnSe PL. First, because the presence of the laser liberates the ethyl radicals from the DEZn, the optical properties of the ZnSe improve. The improvement is manifested by an increase in the ratio of the intensities of the donor-bound exciton feature to the defect band feature. Second, when solid elemental Zn is employed in the growth, the laser desorbs the Se from the surface. The PL properties of the respective films reflect the increase in the concentration of Zn vacancies at the surface by a decrease in the same intensity ratio. Third, when DMZn is employed in the growth, the laser increases the either the impurity concentration or the concentration of vacancies in the film. This reduction is manifested by a delayed appearance of the shallow donor-acceptor pair feature in the PL with respect to increasing growth temperatures. Thererefore, along with affecting the growth rate for MOMBE-grown ZnSe, laser-assisted growth alters the optical properties of the ZnSe.

The PL of doped ZnSe films is sensitive to the mechanism by which the respective dopant is incorporated. For n-type ZnSe, the intensity of the donor-bound exciton increases for increasing chlorine concentrations. However, for p-type ZnSe, the primary PL feature is a DAP transition. The shape of the DAP feature changes for increasing nitrogen concentrations because a deep DAP transition becomes as intense as the shallow DAP transition. Both of the DAP features as well as the corresponding LO phonon replicas for both levels form one unresolved feature for highly doped ZnSe:N. As a result, the relative doping concentration can be estimated using PL.

The PL analysis in this thesis has been dependent upon the availability of enough

ZnSe films grown under fixed conditions to make relevant comparisons. However, in order to separate the relationships between the thickness and the growth temperature to the PL features, a more complete set of data is necessary. Also, the presence of a second DAP level in the PL of MOMBE-grown ZnSe when a DMZn source is used, needs to be investigated further. Finally, the effects of thermally cycling the ZnSe films has not been considered, and there is cause for further investigation. All of the undoped films have been cooled to 10 K for PL measurements several times, with little effect on the PL. However, ZnSe:N has shown a decrease in the intensity of the DAP feature when thermally cycled.

Appendix A: Properties of ZnSe

ZnSe is a II-VI semiconductor, where the group II element is the Zn and the group VI element is the Se. It forms a zinc-blende lattice structure, with a direct energy bandgap. A list of the quantitative properties of ZnSe, and for comparison, GaAs and Si is given in the table below. From the table of material properties, the unique qualities of ZnSe become apparent. In comparison to ZnSe, Si is not a good optical emitter, since it has an indirect energy gap. In addition, for the electron effective mass, Si has both a transverse, (t), and a longitudinal, (l) effective masses. The hole effective mass of Si is given for both the light hole, (lh), and heavy hole, (hh), bands. GaAs and ZnSe are both optical materials (meaning, both have direct energy gaps), with the emission of GaAs in the infrared region and of ZnSe in the blue region of the spectrum. Of the three materials compared in the table, GaAs has the highest mobility, and ZnSe has the lowest. A GaAs/ZnSe heterostructure is a logical combination due to the similar lattice constants. The wide bandgap of ZnSe as compared to GaAs is useful for carrier confinement in a GaAs/ZnSe quantum well structure.

Property	*ZnSe*	*GaAs*	*Si*	*Refs*
Lattice constant Å	5.6676	5.6533	5.4309	[23, 16]
Energy gap (eV)	2.67	1.43	1.11	[16, 23]
Type of transition	direct	direct	indirect	
Electron mobility ($\frac{cm^2}{Vsec}$)	200	8500	1500	[23, 33]
Electron effective mass	0.17	0.067	0.19(t),0.98(l)	[16, 35]
Hole effective mass	0.65	0.082	0.49(hh),0.16(lh)	[34, 23]
Ionicity	0.63	0.31	0	[23]
Dielectric constant	8.1	13.1	11.9	[16, 36]

Appendix B: Substrate Carrier and Wafer Preparation

Substrate Carrier Preparation

A two piece molybdenum block consisting of a rim and a 2 inch insert was used for the II-VI growths. The insert could be removed and replaced with a 2 inch GaAs wafer if desired, but in this investigation the GaAs samples were indium bonded to the molybdenum insert. The pieces of the block are initially cleaned in the same manner, using a standard degrease procedure outlined in the following Table.

Step	*Solvent*	*Process*	*Time (min)*
1	TCA	heat to a boil	10
2	TCA	heat to a boil	10
3	acetone	ultrasonic clean	5
4	acetone	ultrasonic clean	5
5	methanol	ultrasonic clean	5
6	methanol	ultrasonic clean	5

After this procedure, the entire carrier is blown dry with nitrogen. The II-VI block is etched in a bath of 10:1 deionized water and hydrochloric acid to remove any prior mounting material (In or In—Ga) from the surface. Afterwards, the carrier is etched in a 3:1 bath of deionized water and nitric acid for 15-20 seconds followed by hydrochloric acid for 2 minutes. Finally, the block is rinsed thoroughly in deionized water. The II-VI carrier is then baked at 700°C for one hour.

Wafer Preparation

The films are grown on two inch semi-insulating GaAs (001) wafers from Sumitomo. For continuity, the wafer is cleaved into four parts for four separate film growths. There are two stages to the wafer preparation: degrease and etch. The wafer, mounting tools, and eutectics first undergo the same degrease procedure as

the substrate carrier. Afterwards, the wafer is rinsed in deionized water and blown dry with nitrogen. Next, the wafer is etched. The etch process is as follows:

Step	*Chemicals*	*Process*	*Time (sec)*
1	5:1:1 H_2SO_4:H_2O_2:H_2O	mix and rotate	60
2	acid bath	add wafer, rotate	90
3	DI H_2O	rinse wafer	5 min.
4	–	blow dry with nitrogen	–

The etch process removes the top layers (10-15 microns) of the wafer, exposing a clean surface for growth. The rinse step coats the wafer with a new oxide to protect the surface until the sample is in the reactor.

The clean wafer is then mounted onto the substrate carrier using either indium or a gallium/indium alloy. The gallium/indium alloy has the advantage that it is liquid at room temperature and can hence be used for *ex situ* transfers from a III-V sample block to a II-VI sample block.

Bibliography

[1] R. N. Bhargava, "Blue and UV light emitting diodes and lasers," *Optoelectronics,* vol. 7, pp. 19-47, 1992.

[2] M.A. Haase, J. Qiu, J.M. DePuydt, and H. Cheng, "Blue-green laser diodes," *Applied Physics Letters,* vol. 59, p. 1272-1274, 1991.

[3] N. Nakayama, S. Itoh, T. Ohata, K. Nakano, H. Okuyama, M. Ozawa, A. Ishibashi, M. Ikeda, and Y. Mori, "Room temperature continuous operation of blue-green laser diodes," *Electronics Letters,* vol. 29, p. 1488, 1993.

[4] J.M. Gaines, R.R. Drenten, K.W. Haberern, T. Marshall, P. Mensz, and J. Petruzzello, "Blue-green injection lasers containing pseudomorphic $Zn_{1-x}Mg_xS_ySe_{1-y}$ cladding layers and operating up to 394 K," *Applied Physics Letters,* vol. 62, p. 2462-2464, 1993.

[5] E.H.C. Parker, ed The Physics and Technology of Molecular Beam Epitaxy, Plenum Press, New York, 1985.

[6] C.A. Coronado, E. Ho, L.A. Kolodziejski, "Effect of laser on MOMBE of ZnSe using gaseous and solid sources," *Journal of Crystal Growth,* vol.127, pp. 323-326, 1993.

[7] C.A. Coronado, E. Ho, L.A. Kolodziejski, C.A. Huber, "Photo-assisted MOMBE of ZnSe," *Applied Physics Letters,* vol. 61, pp. 534-536, 1992.

[8] E. Ho, C.A. Coronado, L.A. Kolodziejski, "Photo-assisted chemical beam epitaxy of II-VI semiconductors," *Materials Research Society Symposium Proceedings,* vol. 279, pp. 635-644, 1993.

[9] K. Lu, E. Ho, J.L. House, P. Fisher, E. Ho, C. Coronado, G.S. Petrich, L.A. Kolodziejski, "GSMBE Growth of ZnSe on Novel Buffer Layers," *Journal of Vacuum Science Technology,* to be published.

[10] C.A. Coronado, E. Ho, P.A. Fisher, J.L. House, K. Lu, G.S. Petrich, L.A. Kolodziejski, "Gas source molecular beam epitaxy of ZnSe and ZnSe:N," *Journal of Electronic Materials,* to be published.

[11] J.L Beeby, "Theory of RHEED for general surfaces," *Surface Science,* vol. 80, pp. 56-61, 1979.

[12] J.M. Van Hove, P.R. Pukite, and P.I. Cohen, "The dependence of RHEED oscillations on MBE growth parameters," *Journal of Vacuum Science Technology B,* vol. 3, pp. 563-567, 1985.

[13] G.P. Bassini and G.F. Parravicini, Electronic States and Optical Transitions in Solids, Pergamon Press, New York, 1975.

[14] Takafumi Yao, Y. Okada, S. Matsui, K. Ishida, I. Fujimoto, "The effect of lattice deformation on the optical properties and lattice parameters of ZnSe grown on (100)GaAs," *Journal of Crystal Growth,* vol. 81, pp. 518-523, 1987.

[15] K. Shahzad, "Exitonic transitions in ZnSe epilayers grown on GaAs," *Physical Review B,* vol. 38, pp. 8309-8312, 1988.

[16] S.M. Sze, Physics of Semiconductor Devices, Wiley-Interscience, New York, 1981.

[17] T.B. Bateman, H.J. McSkimin and J.M. Whelan, *Journal of Applied Physics,* vol. 30, pp. 544, 1979.

[18] M.E. Straumanis, J.P. Krumme and M. Rubenstein, *Journal of the Electrochemical Society,* vol. 114, pp. 640, 1967.

[19] K. Mohammed, D.A. Cammack, R. Dalby, P. Newbury, B.L. Greenberg, J. Petruzzello, and R.N. Bhargava, "Effect of Lattice Mismatch in ZnSe epilayers grown on GaAs by molecular beam epitaxy," *Applied Physics Letters* vol. 50, pp. 37-39, 1986.

[20] Jacques I. Pankove, Optical Processes in Semiconductors, Dover Publications, New York, 1971.

[21] G.E. Hite, *Physics Review* vol. 156, p. 850, 1967.

[22] G. Kartheuster, Dissertation, Universitat Regensburg, 1973.

[23] E. Kaldis, Current Topics in Materials Science, vol. 9, 1982.

[24] P.J. Dean, D.C. Herbert, "Donor bound-exciton excited states in zinc selenide," *Physical Review B,* vol. 23, pp. 4888-4901, 1981.

[25] Computer software written by Dr. Gale Petrich.

[26] K.P. Giapis, K.F. Jensen, J.E. Potts, and S.J. Pachuta, "Carbon incorporation in ZnSe grown by metalorganic chemical vapor deposition," *Applied Physics Letters,* vol. 55, pp. 463-465, 1989.

[27] J. Reichow, J. Griesche, N. Hoffman, C. Muggelberg, H. Rossmann, L. Wilde, F. Henneberger, and K. Jacobs, "Molecular beam epitaxial growth and characterization of ZnSe and GaAs," *Journal of Crystal Growth,* vol. 131, pp. 277-282, 1993.

[28] Junji Saraie, N. Matsumura, M. Tsubokura, K. Miyagawa, N. Nakamura, "Y-line emission and lattice relaxation in MBE-ZnSe and -ZnSSe on GaAs" *Japanese Journal of Applied Physics,* vol.28, pp. L108-L111, 1989.

[29] A. E. Thomas, G.J. Russell and J. Woods, "Self-activated emission in ZnS and ZnSe," *Journal of Physics C: Solid State Physics,* vol. 17, pp. 6219-6228, 1984.

[30] E. Ho, C.A. Coronado, L.A. Kolodziejski, "Elimination of Surface Site Blockage due to Ethyl Species in MOBME of ZnSe," *Journal of Electronic Materials,* vol. 22, pp. 473-478, 1993.

[31] B.N. Murdin, B.C. Cavenett, C.R. Pidgeon, J. Simpson, I. Hauksson and K.A Prior, "Optically detected magnetic resonance of deep centers in molecular beam epitaxy ZnSe:N," *Applied Physics Letters,* vol. 63, pp. 2411-2413, 1993.

[32] J. Qui, J.M. DePuydt, H. Cheng, and M.A. Haase, "Heavily doped p-ZnSe:N grown by molecular beam epitaxy," *Applied Physics Letters,* vol. 59, p. 2992, 1991.

[33] M. Chandrasekhar and F. H. Pollak, *Physics Review B,* vol. 15, pp. 2127, 1977.

[34] C.M.H. Driscoll, A.F.W. Willoughby, J.B. Mullin and B.W. Straughan, Gallium Arsenide and Related Compounds, Institute of Physics, London, p. 275, 1975.

[35] J.D. Wiley, *Solid State Community,* vol. 8 , pp. 1865, 1970.

[36] B. Hu, A. Yin, G. Karczewski, H. Luo, S. W. Short, N. Samarth, M. Dobrowolska, and J. K. Furdyna, *Journal of Applied Physics,* vol. 74, pp. 4153-4157, 1993.